JCTC Journal of Chemical Theory and Computation

Article

pubs.acs.org/JCTC

Proton/Hydrogen Transfer Mechanisms in the Guanine–Cytosine Base Pair: Photostability and Tautomerism

Vicenta Sauri,*[,†] João P. Gobbo,*[,‡] Juan J. Serrano-Pérez,[§] Marcus Lundberg,[∥] Pedro B. Coto,[†,⊥,#] Luis Serrano-Andrés,[†] Antonio C. Borin,[‡] Roland Lindh,[∥] Manuela Merchán,[†] and Daniel Roca-Sanjuán*[,∥]

[†]Instituto de Ciencia Molecular, Universitat de València, P.O. Box 22085, ES-46071 València, Spain

[‡]Instituto de Química, Universidade de São Paulo and NAP-PhotoTech, the USP Consortium for Photochemical Technology, Av. Prof. Lineu Prestes, 748, 05508-900, São Paulo, SP, Brazil

[§]Department of Chemistry, Imperial College London, Exhibition Road, London, SW7 2AZ, United Kingdom

[∥]Department of Chemistry—Ångström, Theoretical Chemistry Program, Uppsala University, P.O. Box 518, SE-75120 Uppsala, Sweden

[⊥]Institut für Theoretische Physik, Friedrich-Alexander-Universität Erlangen-Nürnberg, Staudtstraβe 7, 91058 Erlangen, Germany

[#]Departamento de Química-Física, Universidad de Alcalá de Henares, Ctra. Madrid-Barcelona (Autovía A2) Km. 33.600, 28871 Alcalá de Henares, Spain

Supporting Information

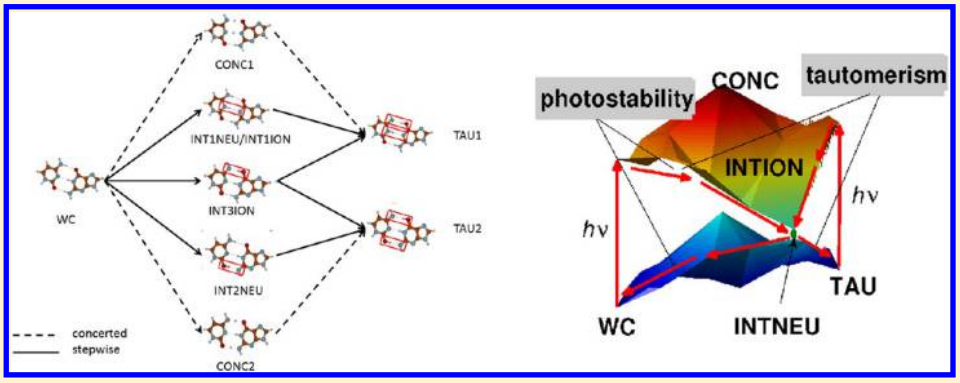

ABSTRACT: Proton/hydrogen-transfer processes have been broadly studied in the past 50 years to explain the photostability and the spontaneous tautomerism in the DNA base pairs. In the present study, the CASSCF/CASPT2 methodology is used to map the two-dimensional potential energy surfaces along the stretched NH reaction coordinates of the guanine–cytosine (GC) base pair. Concerted and stepwise pathways are explored initially *in vacuo*, and three mechanisms are studied: the stepwise double proton transfer, the stepwise double hydrogen transfer, and the concerted double proton transfer. The results are consistent with previous findings related to the photostability of the GC base pair, and a new contribution to tautomerism is provided. The C-based imino-oxo and imino-enol GC tautomers, which can be generated during the UV irradiation of the Watson–Crick base pair, have analogous radiationless energy-decay channels to those of the canonical base pair. In addition, the C-based imino-enol GC tautomer is thermally less stable. A study of the GC base pair is carried out subsequently taking into account the DNA surroundings in the biological environment. The most important stationary points are computed using the quantum mechanics/molecular mechanics (QM/MM) approach, suggesting a similar scenario for the proton/hydrogen-transfer phenomena *in vacuo* and in DNA. Finally, the static model is complemented by *ab initio* dynamic simulations, which show that vibrations at the hydrogen bonds can indeed originate hydrogen-transfer processes in the GC base pair. The relevance of the present findings for the rationalization of the preservation of the genetic code and mutagenesis is discussed.

INTRODUCTION

Since the discovery of the chemical composition of DNA and the associated structural arrangement in a double-helix form,[1,2] the profound understanding of its properties has constituted an intriguing challenge to the scientific community. Thus, DNA and its analogues have been the subject of intensive research in distinct areas of major interest within the realms of nanotechnology,[3] computer sciences,[4] and medicinal chemistry.[5] Special attention has been focused on DNA damage caused by

Received: July 19, 2012
Published: October 15, 2012

dx.doi.org/10.1021/ct3006166 | J. Chem. Theory Comput. 2013, 9, 481–496

UV radiation. Within this context, in order to unveil the operative mechanisms for the formation of lesions and mutations in the genetic code, theoretical and experimental studies have been actively performed.[6−8]

UV radiation can stimulate cycloaddition photoreactions in DNA molecules, generating photodimers and photoadducts.[7,9−11] Among the photodimers (cyclobutane pyrimidine dimers, CPDs), the most common lesion involving a single DNA strand corresponds to the dimerization of two stacked thymine molecules. On the other hand, the cycloaddition of two cytosine molecules known as 6−4 cytosine adducts is the photoadduct of major impact.

Effects of DNA damage can be severe because it may interrupt replication or originate transition or transversion mutations, altering the ordering of the nucleic acid bases (NABs) and therefore modifying the genetic code.[12,13] The tautomeric forms in the guanine−cytosine (GC) base pairs have been recently suggested to be responsible for the universal mutation of guanine−cytosine to adenine−thymine, GC→AT, frequently found in bacteria, fungi, plants, and animals.[14] In order to deal with DNA lesions, nature has developed enzymatic mechanisms, which are involved in the repair process. Enzymatic complexes, such as DNA−glycolases, polymerases, and photolyases, participate in different excision repair mechanisms.[15,16] DNA-photolyases, in particular, require visible light to repair CPD photolesions. The interplay between both mutagenic and DNA-repair processes constitutes the basic framework in which the evolution of life, as we currently know, is feasible.

In the past decade, different research groups have focused on computational studies aiming at understanding the significance of the chemical physical properties of the natural selected canonical NABs, which are more stable than their tautomeric forms, and the underlying mechanisms preserving the genetic code and avoiding mutations.[17−42] It has been demonstrated that the fast deactivation of NABs triggered by UV light absorption is due to a barrierless decay of the bright spectroscopic $\pi\pi^*$ singlet excited state toward the ground state. Femtosecond pump−probe experiments with the canonical NABs showed multi-exponential decay channels in the femtosecond and picosecond time scales, strong evidence for the stability of the natural NABs.[43−46] It is interesting to note that similar experiments with NAB monomers in the aqueous phase provided low fluorescence quantum yields, which suggests that the NABs' ultrashort lifetimes are intrinsic molecular properties.[47−51]

New photochemical paths have been more recently determined in π-stacked NABs,[52−64] which compete with the photostable routes present in the nucleobase monomers and explain the formation of the CPD lesions[59−62,64] found in UV-irradiated DNA polynucleotides.[65] Excited-state dimers of adjacent NABs (bioexcimers) have been shown to be the precursors in the photoreactive process leading to the lesion. Along the main energy-decay pathway of the NAB dimers, energy barriers have been found for cytosine and not for thymine and uracil,[62,64] which agree with the lower quantum yield for the production of the lesion in the former NAB.[63]

It is clear that although relevant information can be obtained from the studies with the isolated NAB monomers and intrastrand π-stacked dimers, further aspects can be understood by exploring the photochemistry of the DNA base pairs, especially those related to the double helix. In 1953, Watson and Crick found the B-DNA structure as the most common arrangement of the genetic code.[2] This structure basically consists of purine (G and A) and pyrimidine (C and T) molecules, arranged in two complementary strands linked by hydrogen bonds, which results in the GC and AT base pairs. The gas-phase experiments carried out by using UV-IR double-resonance techniques on isolated GC base pairs have shown that the Watson−Crick (WC) form (see Figure 1),

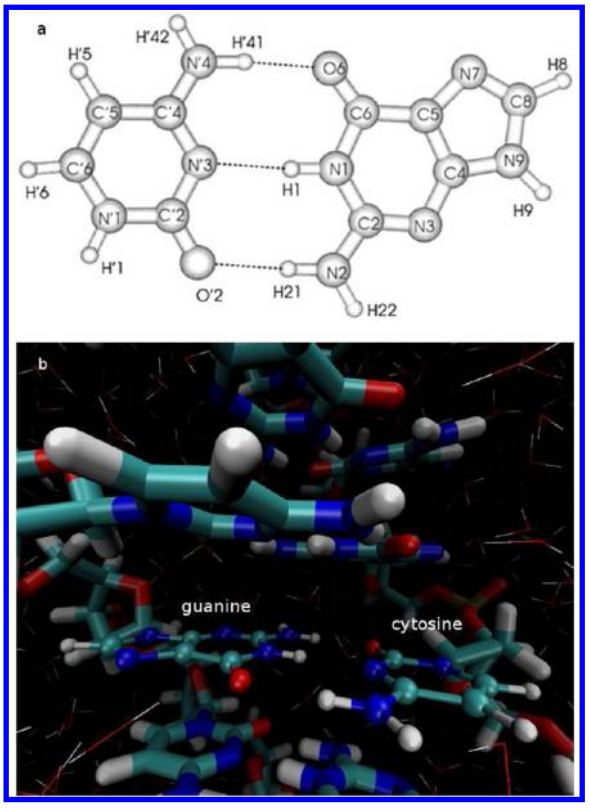

Figure 1. The Watson−Crick GC base pair. (a) Numbering and atom labeling for the GC dimer.[84] (b) Perspective view of the GC base pair in a hydrated DNA double helix of 18 alternating base pairs, namely $d(GC)_9 \cdot d(GC)_9$.

which is the most stable form, has a broad UV absorption spectrum, whereas the non-WC GC base pairs exhibit sharp peaks.[66] Such experimental evidence has been proposed to be connected to the radiationless decay taking place after the UV light absorption of the canonical GC base pair.[66]

Early in 1963, Löwdin introduced the hypothesis that the double proton/hydrogen-transfer reaction in DNA base pairs could be a possible source of spontaneous mutations.[67,68] Since this work, the double proton/hydrogen transfer induced by photoexcitation in model DNA base pairs has been studied both experimental[69−75] and theoretically.[76−79] In order to investigate whether the reaction mechanism is stepwise or concerted, and the nature of the intermediates involved in the process, Kwon and Zewail employed femtosecond dynamic techniques in the study of the 7-azaindole,[74] concluding that the stepwise pathway drawn from early theoretical works[79] is correct.

Double transfer of a proton/hydrogen has also been considered as a possible mechanism to explain the photostability of the WC DNA base pairs.[74,80−83] At first, the proton (H_1) in the central hydrogen-bond network migrates from G to C (see Figure 1). Next, it returns to the purine (G) moiety, which supports the stepwise pathway. Sobolewski, Domcke, and co-workers have proposed that the proton transfer takes place after population of a state of charge transfer (CT) nature in the WC GC base pair.[80−82] The radiationless deactivation could be mediated by a

dx.doi.org/10.1021/ct3006166 | J. Chem. Theory Comput. 2013, 9, 481−496

conical intersection (CI) between the CT state and the ground state, $(S_0/S_1)_{CI}$, taking place while the proton is transferred to the pyrimidine moiety. The charge separation in the ground-state potential energy surface at the $(S_0/S_1)_{CI}$ crossing allows the back transfer of the proton to the purine moiety. The mechanism is known as electron-driven double transfer of a single proton.

Despite the fact that the studies on mimetic models of the GC base pair clearly pointed to an active participation of the proton/hydrogen transfer in the photochemistry of the systems, the relevance of base pairing in the excited-state dynamics of the DNA molecule is still uncertain.[85−96] Shortened fluorescence lifetimes in alternating DNA duplexes poly(dGdC)·poly(dGdC) relative to the G and C mononucleotides have been measured experimentally by using fluorescence upconversion spectroscopy,[86] indicating that proton/hydrogen transfer could be relevant, as suggested by theoretical calculations.[85] On the other hand, transient absorption measurements have shown ground-state recovery in the related $d(GC)_9 \cdot d(GC)_9$ DNA double strand an order of magnitude slower than in the monomeric nucleotides, suggesting excited-state decays driven by the formation of π-stacked excited-state species (or exciplexes) and not *via* interstrand proton/hydrogen transfer.[89] In this line, a combined experimental and time-dependent density functional theory (TD-DFT) study on the GC base pair in solution with $CHCl_3$ has also pointed to a nonefficient process in solution.[96] The authors of this work have also suggested that the photoinduced hydrogen transfer cannot be considered as a relevant deactivation path in DNA. However, the most recent experiments carried out by de La Harpe et al. have reported pronounced isotope effects on the long-lived exciplex excited states of a $d(GC)_9 \cdot d(GC)_9$ double strand,[91] in agreement with independent studies by Doorley et al.[90]

In this scenario, a model based on the full characterization of the energy-decay channels involving proton/hydrogen transfer in the GC base pair seems timely in order to establish the operative mechanisms for photostability and tautomerism and to shed light into the relevance of base-pairing in the photodynamics of DNA. Especially important shall be certain aspects related to the photochemical channels connecting the WC base pair with other tautomeric configurations. The energy-decay paths of the noncanonical species have not been previously explored. Knowledge about those new photochemical routes might be valuable for the interpretation of experimental observations. Hence, in the present contribution, the proton/hydrogen transfer of the isolated GC base pair in the excited state is studied by mapping the two-dimensional potential energy surfaces (PESs) along the hydrogen-bond reaction coordinates, evaluating different possible competitive deactivation pathways. The main equilibrium structures for the double proton/hydrogen phenomena in the isolated GC base pair are also characterized in a DNA double helix of 18 alternating GC base pairs in water (see Figure 1b), which allow comparisons with previous experiments on DNA duplexes with the same nucleotide sequence. Such a static study is additionally extended with some dynamical insights. Previous work on the dynamics of the system has been reported, although at levels of theory not able to describe the overall photochemistry of the GC base pair.[85,93]

The subsequent parts of the paper are structured as follows: methods, results and discussion, and summary and concluding remarks.

COMPUTATIONAL METHODS

Below, we first describe the strategies designed to explore the energy-decay routes of the GC base pair. Next, the methods employed to characterize the electronic structure and the computational techniques used in the semiclassical dynamics calculations are explained in detail.

The Energy-Decay Paths of the GC Base Pair. Ground as well as excited states of LE (locally excited) and CT character are described. Both stepwise and concerted pathways are considered in a schematic manner as shown in Figure 2. In short, the canonical base pair, hereafter WC, at the ground-state equilibrium geometry absorbs UV radiation. In the Franck−Condon (FC) region, the energy is transferred to the low-lying $^1\pi\pi^*$ bright state. Two tautomeric configurations of the base pair can be potentially formed from this point depending on the hydrogen bonds involved in the proton/hydrogen-transfer processes. Whereas a double proton/hydrogen transfer at the $N'_3\cdots H_1N_1$ and $N_4'H_{41}'\cdots O_6$ sites might result in the 9H-2-amino-6-hydroxypurine/3H-2-oxo-4-iminopyrimidine or C-based imino-oxo tautomers (hereafter, TAU1), the 1H-9H-2-imino-6-hydroxypurine/2-hydroxy-4-iminopyrimidine or C-based imino-enol base-pair configuration (hereafter, TAU2) can be produced after an analogous process at the $O'_2\cdots H_{21}N_2$ and $N_4'H_{41}'\cdots O_6$ sites. In the concerted or symmetric pathway, the H atoms are transferred synchronously (CONC1 and CONC2), connecting the canonical GC base pair and the respective tautomeric form as shown in Figure 2. Meanwhile, two asymmetric pathways, *via* intermediates of a different nature (either neutral or ionic), can be relevant to the photochemistry of the dimer. The neutral species (INT1NEU and INT2NEU) feature a CT electronic structure, whereas the ionic ones (INT1ION and INT3ION) correspond to LE excitations.

Electronic Structure. Characterization of the lowest-lying singlet $\pi\pi^*$ excited states of the GC base pair has been performed with the complete-active-space self-consistent-field second-order perturbation theory (CASPT2) method,[97−101] as implemented in the MOLCAS-7 package,[102] and the one-electron double-ζ plus polarization atomic natural orbital basis set with the primitive set C,N,O(10s6p3d)/H(7s3p), the ANO-S set,[103] contracted to C,N,O[3s2p1d]/H[2s1p]. A set of restricted active space second-order perturbation theory (RASPT2) calculations up to quadruple excited configurations has been initially carried out in the canonical GC base pair and the tautomer TAU1 in order to determine the main lowest-lying excited states that are involved in the photochemistry of GC. With the RAS2 subspace empty, the valence π (RAS1) and π^* (RAS3) molecular orbitals (MOs) have been employed in the calibration calculations.[104] A six-root state average SA(6)-RASSCF/RASPT2 has been performed for the $\pi\pi^*$ states, whereas a four-root state average SA(4)-RASSCF/RASPT2 was chosen to compute $n\pi^*$ states. The highest energy $\pi\pi^*$ states have been found at 5.20 and 5.53 eV for the canonical GC base pair and the tautomeric form, respectively. On the other hand, employing the same structures, the lowest-energy $n\pi^*$ states have been placed at 5.91 and 5.90 eV. It consequently implies that in order to examine the photochemistry of GC just the $\pi\pi^*$ excited states have to be considered. Accordingly, the active space selected for the CASSCF/CASPT2 calculations comprises 12 π valence electrons distributed into 12 π active MOs [(hereafter, CASSCF/CASPT2(12,12)], excluding the remaining occupied and unoccupied MOs with highest and lowest occupation numbers, respectively, in the RASSCF computations (see Figure S1). A C_s symmetry constraint has been imposed in the CASSCF geometry optimizations and CASPT2 vertical energies. This approach will not allow us to describe properly processes which involve out-of-plane geometry distortions, such as the decay paths localized on the nucleobases. However, it is reasonable for characterizing the photoinduced proton/hydrogen transfer,

dx.doi.org/10.1021/ct3006166 | J. Chem. Theory Comput. 2013, 9, 481−496

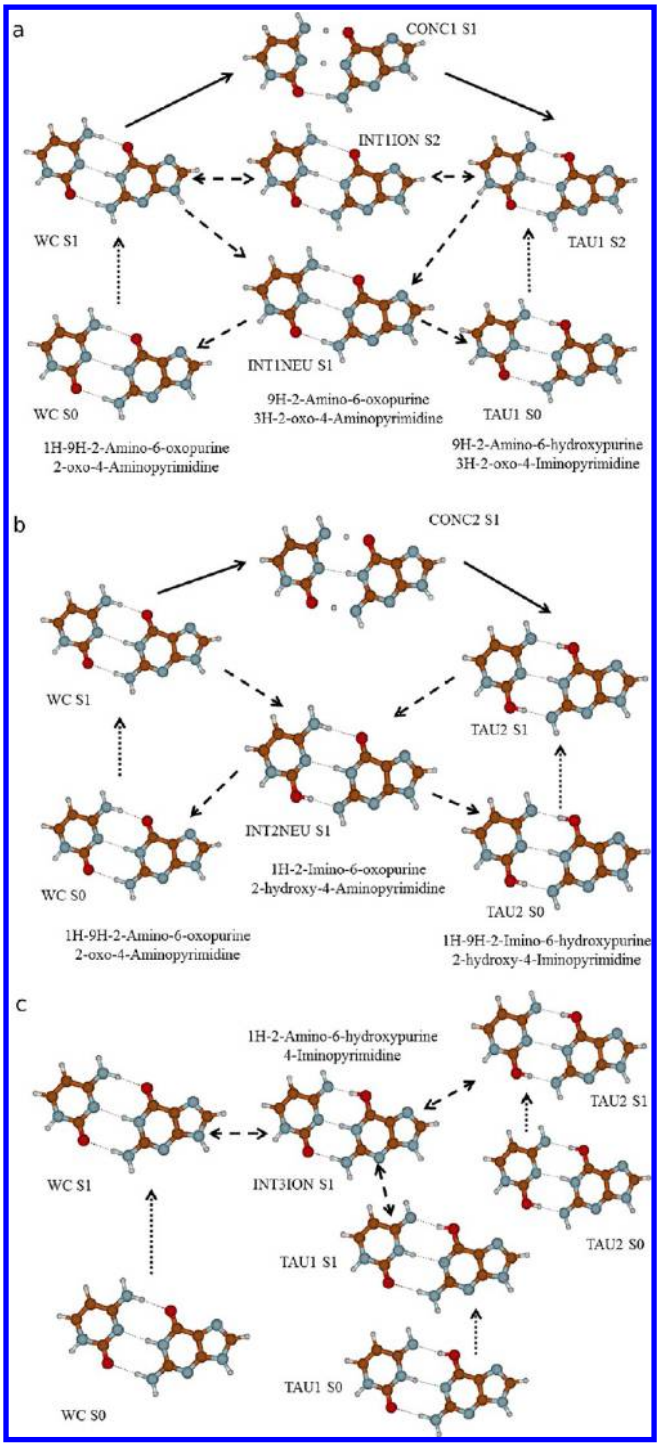

Figure 2. Scheme of the paths explored for the excited state double proton/hydrogen-transfer process in the GC base pair. The atoms transferred are H_1 in G plus H_{41}' of the amino group in C (a), H_{21} and H_{41}' of the amino groups in both G and C (b), and H_{41}' in the amino group of C plus either H_1 or H_{21} in G (c). The tautomers TAU1 and TAU2 are originated *via* these H-transfer processes. Paths can be concerted (CONC1 and CONC2) or stepwise *via* neutral (INT1NEU and INT2NEU) or ionic (INT1ION and INT3ION) intermediates. The electronic state related to each one of the GC forms is shown in advance (S_0, S_1, and S_2 stand for the ground and two lowest-lying excited states). Symmetric and asymmetric C_s paths are represented by solid and dashed arrows, respectively, while absorption processes are shown in dotted arrows.

as has been previously shown in the excited state proton/hydrogen transfer in the AT base pair[105] and the 7-azaindole dimer.[79]

In addition, the presence of an equilibrium structure on an excited state of LE character can be used within the present approach to predict a possible deactivation channel through the monomer. Two-dimensional PESs have been mapped along the reaction coordinates at the CASPT2 level by using linear interpolation in internal coordinates (LIIC) among the WC, the intermediates (INT1NEU, INT2NEU, INT1ION, and INT3ION), and the tautomeric (TAU1 and TAU2) GC base-pair forms. Oscillator strengths have been computed from CASSCF dipole moments and CASPT2 energies. The conventional CASPT2 method has been employed (IPEA = 0.0 au).[97] In order to minimize weakly interacting intruder states, the imaginary level-shift technique with a parameter of 0.2 au has been used.[106] Unless otherwise stated, the CASSCF/CASPT2 calculations have been performed as a state average CASSCF procedure of six roots [SA(6)-CASSCF]. In some cases, 10 roots have been required in order to find the relevant states at high energy, showing energy differences at the CASPT2 level lower than 0.1 eV, or 0.2 eV in a few cases, with respect to the SA(6)-CASSCF/CASPT2 results, which is within the error of the method.

The hybrid quantum mechanics/molecular mechanics (QM/MM) approach has been used to simulate the biological environment in the DNA surroundings. As the QM core, the GC base pair (see Figure 1b) has been modeled by means of the *ab initio* CASSCF/CASPT2 method, using the same SA-CASSCF average procedure, active space, basis set, and symmetry constraint as in the in vacuo computations. The MM subsystem has been represented by using the AMBER99 force field[107,108] in order to include the double helix strand, the aqueous media, and the external counterions. The double helix is composed of 18 alternating GC base pairs and the DNA backbone of deoxyriboses and phosphates [$d(GC)_9 \cdot d(GC)_9$]. The aqueous medium is modeled by an octahedron box of 8618 water molecules surrounding the simulated DNA molecule, and the external counterions are represented by Na^+ monovalent cations. The initial structure employed in the QM/MM computations has been generated by using classical molecular dynamics (MD) simulations (see SI). The employed QM/MM approach takes into account the explicit electronic polarization of the base pair by the DNA double helix and the solvent. Geometry optimizations of the most important stationary points have been performed at the CASSCF/MM level for the GC base pair of interest, the related deoxyribose and phosphate groups, the adjacent nucleotides, and all the water molecules and Na^+ ions within a radius of 5 Å from the QM part. This allows for mutual geometric polarization between the QM moiety and its immediate surroundings. The CASPT2 energies of the lowest-energy states have been compared with the energy values obtained *in vacuo*.

Semiclassical Dynamics. Born−Oppenheimer dynamics calculations have been performed on the excited-state surface of the isolated GC base pair with the MOLCAS-7 program.[102] Newton's equations have been solved by the velocity-Verlet algorithm[109] with a 1 fs time step. Analytical gradients have been computed on-the-fly at the SA(6)-CASSCF(12,12)/ANO-S C,N,O[3s2p1d]/H[2s1p] level of theory with the constraint of C_s symmetry.[110] A group of 300 initial conditions has been generated with the NEWTON-X program,[111] according to the Wigner distribution for the quantum harmonic oscillator,[112] and using the normal modes computed at the B3LYP/6-31G* level of theory with the GAUSSIAN-09 software package.[113] From these data, four representative sets of starting nuclear coordinates and momenta have been selected for subsequent dynamics simulations. The criteria for the selection have been to choose sets,

dx.doi.org/10.1021/ct3006166 | J. Chem. Theory Comput. 2013, 9, 481−496

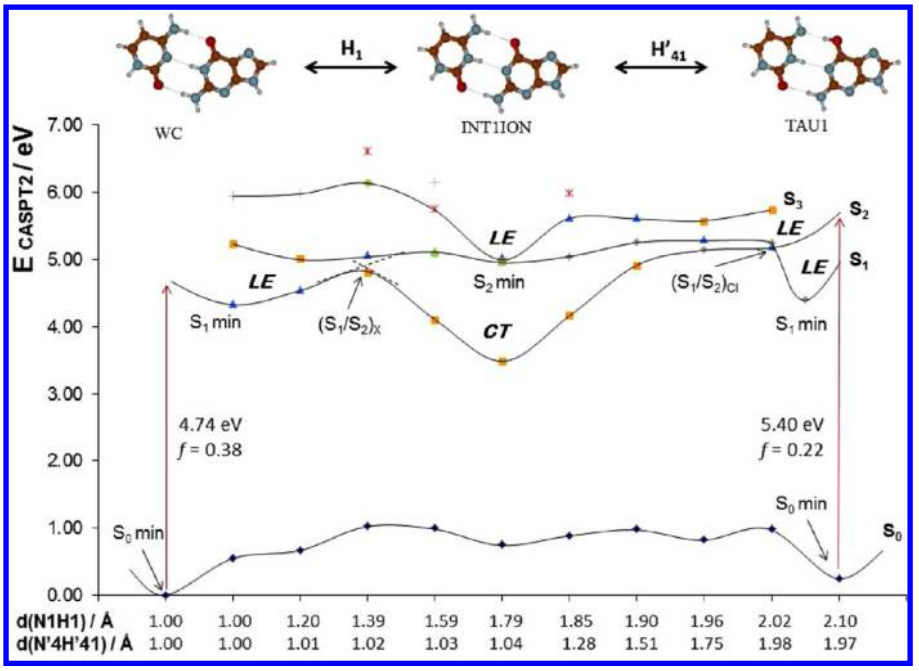

Figure 3. SDPT mechanism (H_1, H_{41}'). GC-base-pair adiabatic PESs of the ground state (S_0) and the low-lying $\pi\pi^*$ singlet excited states (S_1, S_2, and S_3) are mapped at the CASPT2 level along the N_1H_1 and $N_4'H_{41}'$ reaction coordinates, between the WC and TAU1 structures, and *via* the INT1ION intermediate [equilibrium structure of the locally excited S_2 state (S_2 min)]. The computed stationary points for the ground (S_0 min) and excited (S_1 min and S_2 min) states are shown. The CASSCF geometry optimization of the S_4 state for the INT1ION species is the S_2 state at the CASPT2 level. The excited states show either charge transfer (CT), intraguanine locally excited (GG), or intracytosine locally excited (CC) character. To track the nature of states, the dots on the graphics are drawn as follows: blue diamonds, ground state; blue triangles, 1GG; orange squares, 1CT; red asterisks, 2CT; green circles, 3CT; pink crosses, 1CC; gray diamonds, 2GG; yellow squares, 3GG; and violet crosses, 2CC. Energy values are compiled in Table S2.

with initial NH bond distances and scalar projections of the velocities of the H atoms along the interbase-pair hydrogen bonds, which potentially exhibited some of the dynamical aspects of the different relaxation mechanisms earlier established by the static models presented in this study. Bond lengths and velocity values for all the generated initial conditions are displayed in Figures S2−S7.

RESULTS AND DISCUSSION

The photochemistry of the DNA GC base pair is described here in three sections. First, the mechanisms for proton/hydrogen transfer in the isolated GC system will be explained, focusing on the relevant routes for energy decay, the intermediates involved, and the photochemical channels for tautomer formation. Next, the main features of the mechanisms established *in vacuo* will be analyzed in the DNA-embedded GC base pair. Finally, the dynamical properties of the excited-state proton/hydrogen-transfer processes will be presented.

Mechanisms of Photostability and Tautomers Production in the Isolated GC Base Pair. The equilibrium structures for the ground (S_0) and lowest-lying $^1\pi\pi^*$ excited states of the canonical (WC), tautomeric (TAU1 and TAU2), and intermediate (INT1ION, INT3ION, INT1NEU, and INT2NEU) forms of the GC base pair have been obtained with the CASSCF method (see optimized hydrogen-bond distances in Table S1). The mapping of the PESs connecting these points at the CASPT2 level (Figures 3−9) accounts for a qualitative picture of the competitive pathways for energy decay *via* proton/hydrogen transfer in the GC base pair. To determine the two-dimensional PESs, adiabatic curves are depicted. The excited states involve singlet LE and CT excitations, and within the former, both intraguanine GG and intracytosine CC electronic transitions are identified. See more details in section E of the SI and energy values for all the computed states in Tables S2−S8.

The photochemistry of the GC base pair starts with the absorption of UV light. At the FC region of the WC base pair, the brightest low-lying $^1\pi\pi^*$ state (oscillator strength f = 0.38) present a LE excitation on the G moiety with a vertical energy of 4.74 eV (see Figures 3−9). From this point, the system will evolve toward the LE minimum (S_1 min) placed at 4.35 eV. According to previous theoretical studies on the isolated G base, out-of-plane distortions in the six-member ring of G take place along the minimum energy path on the $^1\pi\pi^*$ excited state reaching a CI with the ground state that mediates the nonradiative energy decay of the monomer.[32,35,37−39,42] In the GC base pair, however, the presence of the complementary NAB opens new photochemical paths for deactivating the energy excess after UV irradiation, as was postulated initially by Sobolewski and Domcke[82] and will be analyzed here. On the basis of the present CASSCF/CASPT2 findings, three mechanisms are introduced for the photochemistry of GC in the gas phase: a *stepwise double proton transfer (SDPT)*, a *stepwise double hydrogen transfer (SDHT)*, and a *concerted double proton transfer (CDPT)*. Their relevance in the energy deactivation processes which follow the UV-irradiation of the dimer depends on the topology of the PESs along the reaction paths.

Stepwise Double Proton-Transfer (SDPT) Mechanism. The LE excitation on the G nucleobase is proposed as the driver of the photochemistry in this mechanism. Due to the local character of the excitation, the species exchanged between the NABs are protons (not hydrogen). Three possible combinations of double proton transfer can take place under these conditions, which involve different hydrogen bonds, as depicted in Figures 3−5 and explained in the following.

dx.doi.org/10.1021/ct3006166 | J. Chem. Theory Comput. 2013, 9, 481−496

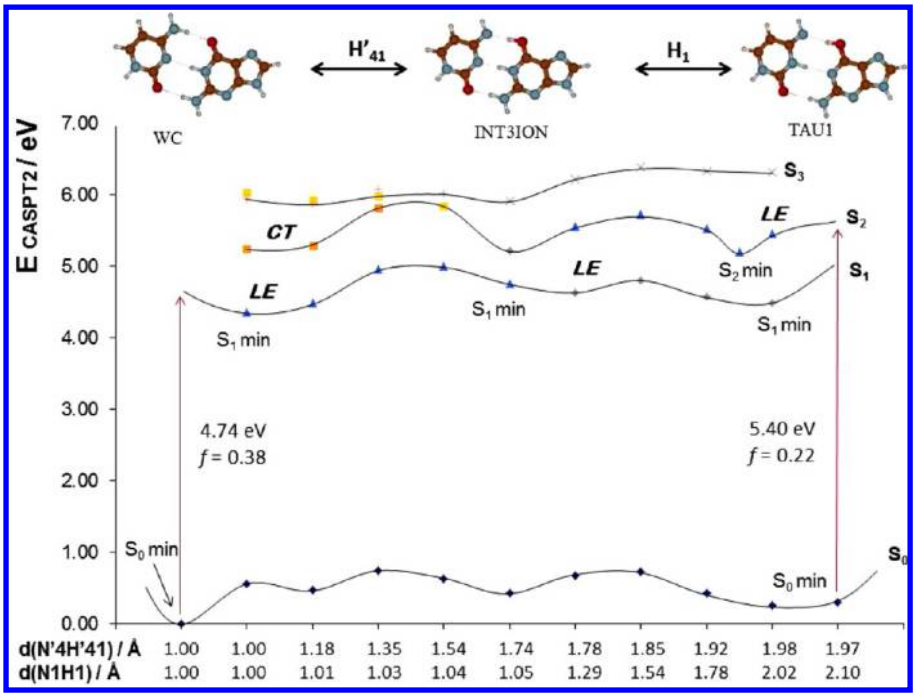

Figure 4. SDPT mechanism (H_{41}', H_1). GC-base-pair adiabatic PESs of the ground state (S_0) and the low-lying $\pi\pi^*$ singlet excited states (S_1, S_2, and S_3) are mapped at the CASPT2 level along the $N_4'H_{41}'$ and N_1H_1 reaction coordinates, between the WC and TAU1 structures, and *via* the INT3ION intermediate [equilibrium structure of the locally excited S_1 state (S_1 min)]. The computed stationary points for the ground (S_0 min) and excited (S_1 min) states are shown. Color code follows that in Figure 3. Energy values are compiled in Table S3.

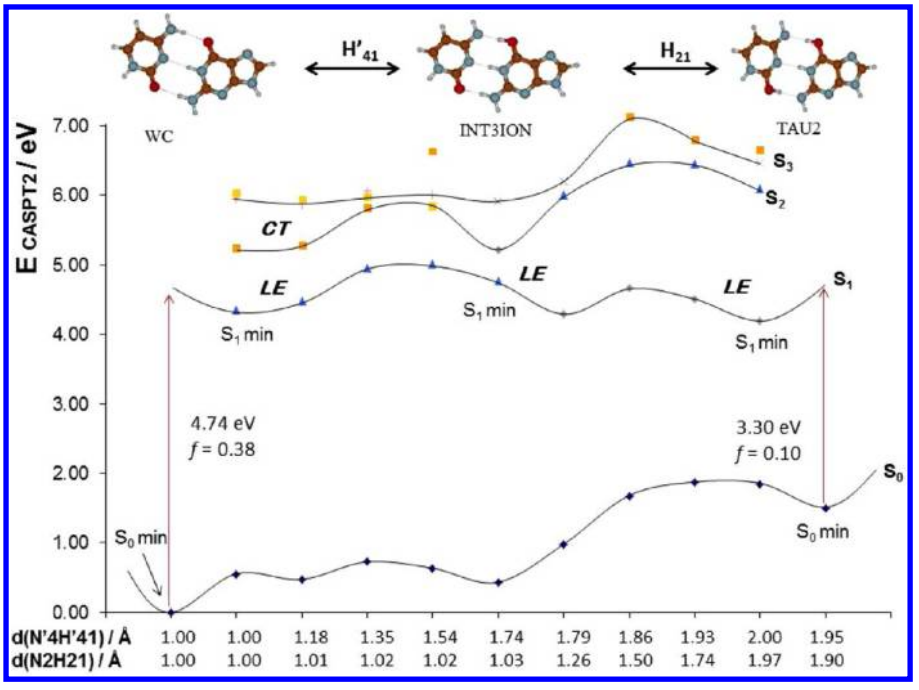

Figure 5. SDPT mechanism (H_{41}', H_{21}). GC-base-pair adiabatic PESs of the ground state (S_0) and low-lying $\pi\pi^*$ singlet excited states (S_1, S_2, and S_3) are mapped at the CASPT2 level along the $N_4'H_{41}'$ and N_2H_{21} reaction coordinates, between the WC and TAU2 structures, and *via* the INT3ION intermediate [equilibrium structure of the locally excited S_1 state (S_1 min)]. The computed stationary points for the ground (S_0 min) and excited (S_1 min) states are shown. Color code follows that in Figure 3. Energy values are compiled in Table S4.

In Figure 3, the PESs are determined through the ionic intermediate INT1ION, whose structure corresponds to the equilibrium structure of the S_2-LE state (S_2 min). The H_1 center proton in G is first transferred to C, therefore generating a charge separation between the monomers. Due to the electrostatic attraction, the NABs approach each other (see CASSCF optimized bond distances in Table S1). A second proton is transferred from the amino group of C to G in order to connect the WC structure with the first tautomeric form (TAU1). It is worth noting that the state with CT nature (S_1) is more stable than the LE state (S_2) at the optimized geometry of the latter around the INT1ION region. This evidence the relevance of the

dx.doi.org/10.1021/ct3006166 | J. Chem. Theory Comput. 2013, 9, 481−496

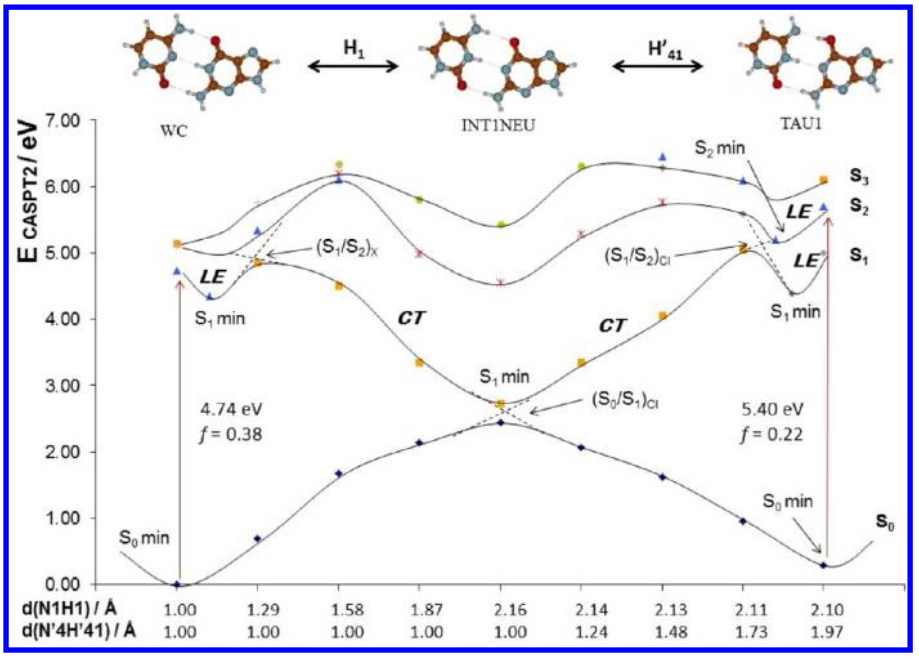

Figure 6. SDHT mechanism (H_1, H_{41}'). GC-base-pair adiabatic PESs of the ground state (S_0) and the low-lying $\pi\pi^*$ singlet excited states (S_1, S_2, and S_3) are mapped at the CASPT2 level along the N_1H_1 and $N_4'H_{41}'$ reaction coordinates, between the WC and TAU1 structures, and *via* the INT1NEU intermediate [equilibrium structure of the charge transfer S_1 state (S_1 min)]. The computed stationary PES points for the ground (S_0 min) and excited (S_1 min and S_2 min) states are shown. Color code follows that in Figure 3. Energy values are compiled in Table S5.

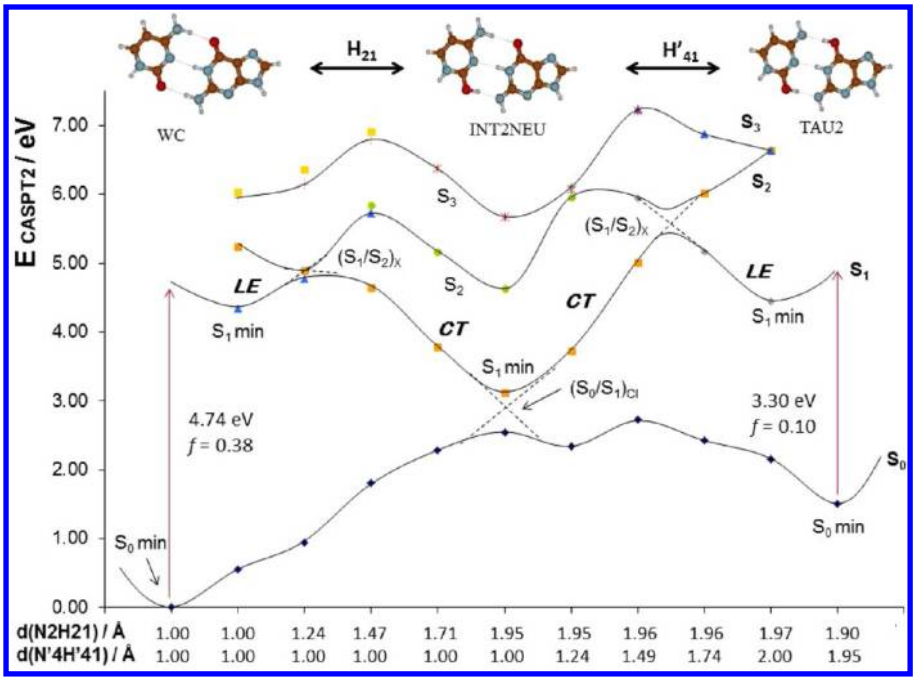

Figure 7. SDHT mechanism (H_{21}, H_{41}'). GC-base-pair adiabatic PESs of the ground state (S_0) and the low-lying $\pi\pi^*$ singlet excited states (S_1, S_2, and S_3) are mapped at the CASPT2 level along the N_2H_{21} and $N_4'H_{41}'$ reaction coordinates, between the WC and TAU2 structures, and *via* the INT2NEU intermediate [equilibrium structure of the charge transfer S_1 state (S_1 min)]. The computed stationary points for the ground (S_0 min) and excited (S_1 min) states are shown. Color code follows that in Figure 3. Energy values are compiled in Table S6.

CT excitation in the radiationless deactivation pathways, as shall be shown below.

In Figure 4, the H_{41}' off-center proton is transferred initially from C to G, resulting in the INT3ION intermediate. This structure is connected to TAU1 by means of a second proton transfer along the $N'_3\cdots H_1N_1$ hydrogen bond. The S_1 PES is relatively flat between the WC and TAU1 configurations. In fact all the WC, INT3ION, and TAU1 S_1 minima (S_1 min) are placed within an energy range of 0.41 eV. Hence, the tautomers formation in the excited-state PES *via* the SDPT mechanism is possible. Once in the S_1 state at the TAU1 region, the system may decay *via* an internal conversion process through the CI of the 9H-6OH-guanine monomer. As previously described by Serrano-Andrés et al.,[37] larger decay times are expected for this deactivation with respect to the G nucleobase due to the presence of barriers along the decay path in the former species

dx.doi.org/10.1021/ct3006166 | J. Chem. Theory Comput. 2013, 9, 481−496

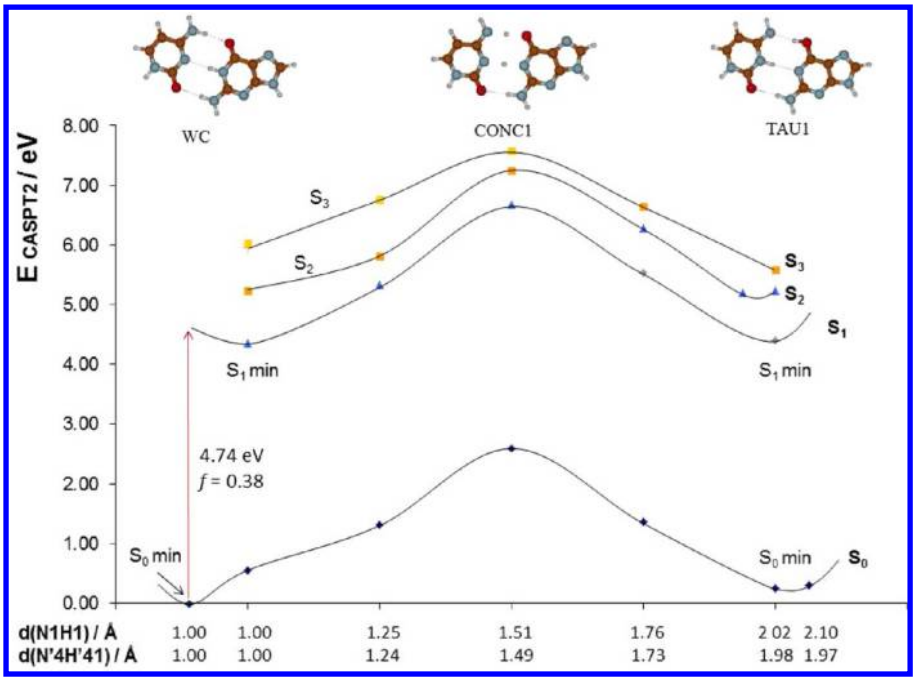

Figure 8. CDPT mechanism (H_1+H_{41}'). GC-base-pair adiabatic PESs of the ground state (S_0) and the low-lying $\pi\pi^*$ singlet excited states (S_1, S_2, and S_3) are mapped at the CASPT2 level along the N_1H_1 and $N_4'H_{41}'$ reaction coordinates, between the WC and TAU1 structures, and *via* the concerted pathway. The computed stationary points for the ground (S_0 min) and excited (S_1 min) states are shown. Color code follows that in Figure 3. Energy values are compiled in Table S7.

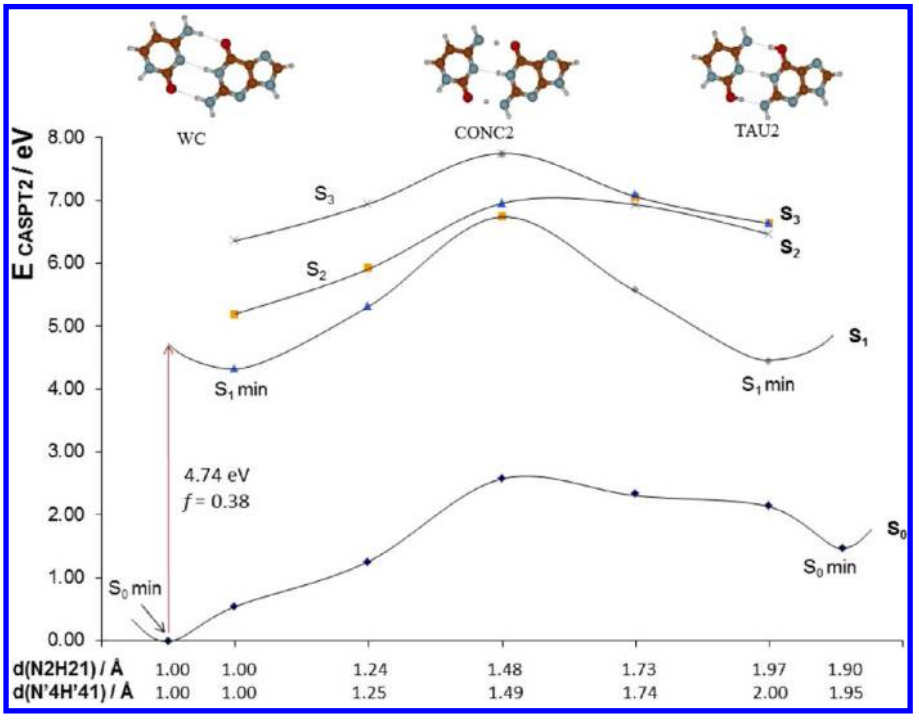

Figure 9. CDPT mechanism (H_{21}+H_{41}'). GC-base-pair adiabatic PESs of the ground state (S_0) and low-lying $\pi\pi^*$ singlet excited states (S_1, S_2, and S_3) mapped at the CASPT2 level along the N_2H_{21} and $N_4'H_{41}'$ reaction coordinates, between the WC and TAU2 structures, and *via* the concerted pathway. The stationary PES points for the ground (S_0 min) and excited (S_1 min) states are shown. Color code follows that in Figure 3. Energy values are compiled in Table S8.

not found in the canonical NAB. The TAU1 base pair, which has a ground-state equilibrium energy just slightly above the canonical GC base pair (0.30 eV; cf. Figures 3 and 4), being therefore relatively stable, does not cause DNA replication breakdowns. However, it might lead to the AT base-pair transition mutation.[67]

In Figure 5, the second tautomeric form (TAU2) is connected with the INT3ION intermediate by means of a second proton transfer from the amino group of G to the oxygen of C. The computed results for the S_1 PES also suggest the formation of tautomers in the excited state, in this case, the TAU2 species. Similarly to TAU1, a CI localized in the 1H-2NH-6OH-guanine

dx.doi.org/10.1021/ct3006166 | *J. Chem. Theory Comput.* 2013, 9, 481−496

monomer might also be expected to mediate a nonradiative energy decay of this modified NAB.[37] Conversely, the ground state of TAU2 is high in energy (1.50 eV), and low energy barriers are found in S_0, which makes the TAU2 species prone to thermal conversions the WC form (cf. Figure 5). This property is highly important for the stability of the genetic code, since the formation of TAU2 can stop the DNA replication (the tautomers in TAU2 cannot match with canonical NABs, unlike those present in TAU1).[67]

Stepwise Double Hydrogen-Transfer (SDHT) Mechanism. The key electronic structure within the basis of this mechanism is a CT excitation from G to C. Therefore, the effective hydrogen transfer implies a proton transfer coupled to an electron exchange in the same direction The initial hydrogen transfer takes place at the hydrogen bond $N'_3\cdots H_1N_1$ or $O'_2\cdots H_{21}N_2$, giving rise to neutral intermediates (see Figure 6 or 7, respectively).

The equilibrium structure of the state with CT character at the GC configuration in which the H_1 atom is transferred to C (INT1NEU) appears in the region of near-degeneracy between the S_0 and S_1 PESs (see Figure 6). In a recent study on the proton/hydrogen-transfer processes in the AT base pair, in which the same methodology and computational strategy as in the present study was used, the CI crossing between both ground and S_1-CT states was optimized, and it was found very close in energy and geometry to the corresponding intermediate.[105] Other computational works have also pointed to the existence of this CI in AT.[114,115] The present study indicates that the situation is the same for GC. Along the S_1 surface that connects the WC and INT1NEU structures, the excited state changes its nature from LE to CT, passing the $(S_1/S_2)_X$ avoided crossing characterized previously by Sobolewski, Domcke, and co-workers.[80,81] From this structure, a barrierless pathway toward the crossing with the ground state, $(S_0/S_1)_{CI}$, is obtained, in agreement with previous results.[80] Both the $(S_1/S_2)_X$ and $(S_0/S_1)_{CI}$ crossings imply an electron transfer process which is the driving force for proton transfer. In the first case, the electron is transferred from G to C, consistent with the lower ionization potential of G relative to C.[116] The charge separation between both NABs, G^+C^-, promotes a proton migration from G to C as shown in Figure 6. In the second crossing $[(S_0/S_1)_{CI}]$, the electron transfer occurs from C to G, G^-C^+, allowing a second proton transfer in the same direction. The proton transferred can be either the same, hence opening a photostable channel in the GC base pair, as established previously,[80,81] or a proton from the amino group of C migrating to G, producing in this case the TAU1 form. In the overall process, two hydrogen atoms have been transferred.

A novel contribution of this study is the mechanism established for the tautomerism of the GC base pair and how it is also photoreversible in the same manner as the canonical GC base pair. At the S_0 optimized geometry of the tautomer, the brightest low-lying $^1\pi\pi^*$ state (oscillator strength $f = 0.22$) is S_2, placed at 5.40 eV and with a LE nature. Proton motions at the $N_4'H_{41}'\cdots O_6$ hydrogen bond can activate a barrierless nonadiabatic process from the brightest S_2-LE state to the S_1-CT state *via* the $(S_1/S_2)_{CI}$ crossing. Once in S_1, the charge separation between both monomers forces the H_{41}' atom to be completely transferred from G to C, yielding the INT1NEU intermediate. Thus, the $(S_0/S_1)_{CI}$ region which mediates the photostability of the WC GC base pair is also reached in the case of the tautomer, funneling the energy to the ground-state equilibrium structure of either the tautomeric form or the canonical GC base pair.

In Figure 7, the SDHT mechanism is analogous to the previous one displayed in Figure 6, although in this case the photostable process takes place *via* the INT2NEU intermediate, and the tautomeric configuration that can be formed as a product of the photoreaction is TAU2. Briefly, at the FC region, the low-lying brightest S_1 state with LE nature can evolve adiabatically (on the S_1 surface) to the region of CT character *via* the $(S_1/S_2)_X$ avoided crossing. Then, the system will be driven toward the $(S_0/S_1)_{CI}$ crossing, and subsequently the WC configuration will be restored (photostable channel) or the tautomer TAU2 will be produced (phototautomerization reaction). Lower energy (3.30 eV) with respect to TAU1 (5.40 eV) is required to populate the brightest low-lying excited state of TAU2 at the FC geometry and therefore to activate the photoinduced conversion toward the WC. These results imply that TAU2 is photochemically less stable than TAU1. The energy-decay mechanism is analogous to the one described for TAU1. Hence, in the vicinity of the FC structure of TAU2, $N_4'H_{41}'$ nuclear vibrations along the hydrogen bond allow the excited-state LE→CT adiabatic conversion toward the INT2NEU form. This intermediate is located in the region of near-degeneracy between the S_0 and S_1 PESs, $(S_0/S_1)_{CI}$. Thus, the excess energy can potentially be funneled to the ground-state minima of either WC or TAU2.

In general, the excited WC, TAU1, and TAU2 species are interconnected to their ground states *via* the SDHT mechanism through nonadiabatic processes. This points to a nonunique ultrafast nonradiative decay channel for the WC form, in contrast to previous proposals.[66,80] Instead, the triple hydrogen-bonding network present in the WC, TAU1, and TAU2 GC configurations provides common deactivation routes *via* hydrogen transfer. Therefore, ultrafast conversions among the canonical and noncanonical forms can be expected during the UV irradiation of the GC base pair.

Concerted Double Proton-Transfer (CDPT) Mechanism. SDPT and SDHT mechanisms involve two steps in which one proton/hydrogen per step is exchanged between the NABs *via* an intermediate. The synchronous proton transfer along the hydrogen bonds also connects the WC configuration with the TAU1 and TAU2 forms (see Figures 8 and 9, respectively). However, high energy barriers are found on the excited state PESs, which makes the concerted mechanism clearly unfavorable for the UV-activated double proton transfer. In addition, ground-state PESs show larger activation barriers, which reduce the significance of the thermal conversion process, in favor of the SDPT mechanism (cf. Figures 8 and 9 vs Figures 3−5).

GC Base Pair in the Biological Environment. SDHT has been established in the preceding section as an efficient mechanism for nonradiative energy decay toward either the canonical GC or the tautomeric form. The process involves states of CT nature and ionic species which are sensitive to solvent interactions. In fact, a clear energy separation between the ground and lowest-lying LE and CT states along the N_1H_1 reaction coordinate was determined by Biemann et al. in a recent TD-DFT study on the GC base pair in solution with $CHCl_3$. This is fully consistent with the fact that the ground state is ionic at the geometry of the intermediates, whereas S_1 is neutral. On the basis of their findings, Biemann et al. have concluded that the hydrogen transfer is not efficient in $CHCl_3$ and cannot be considered to be a relevant deactivation channel in DNA.[96] However, the conditions in which NABs are present in nucleic acids (inner part of the double strand, surrounded by the sugar−phosphate backbone) are different from solution, and comparisons are not straightforward.

To clarify these aspects, we analyze in this section the differences between the SDPT and SDHT mechanisms in the gas

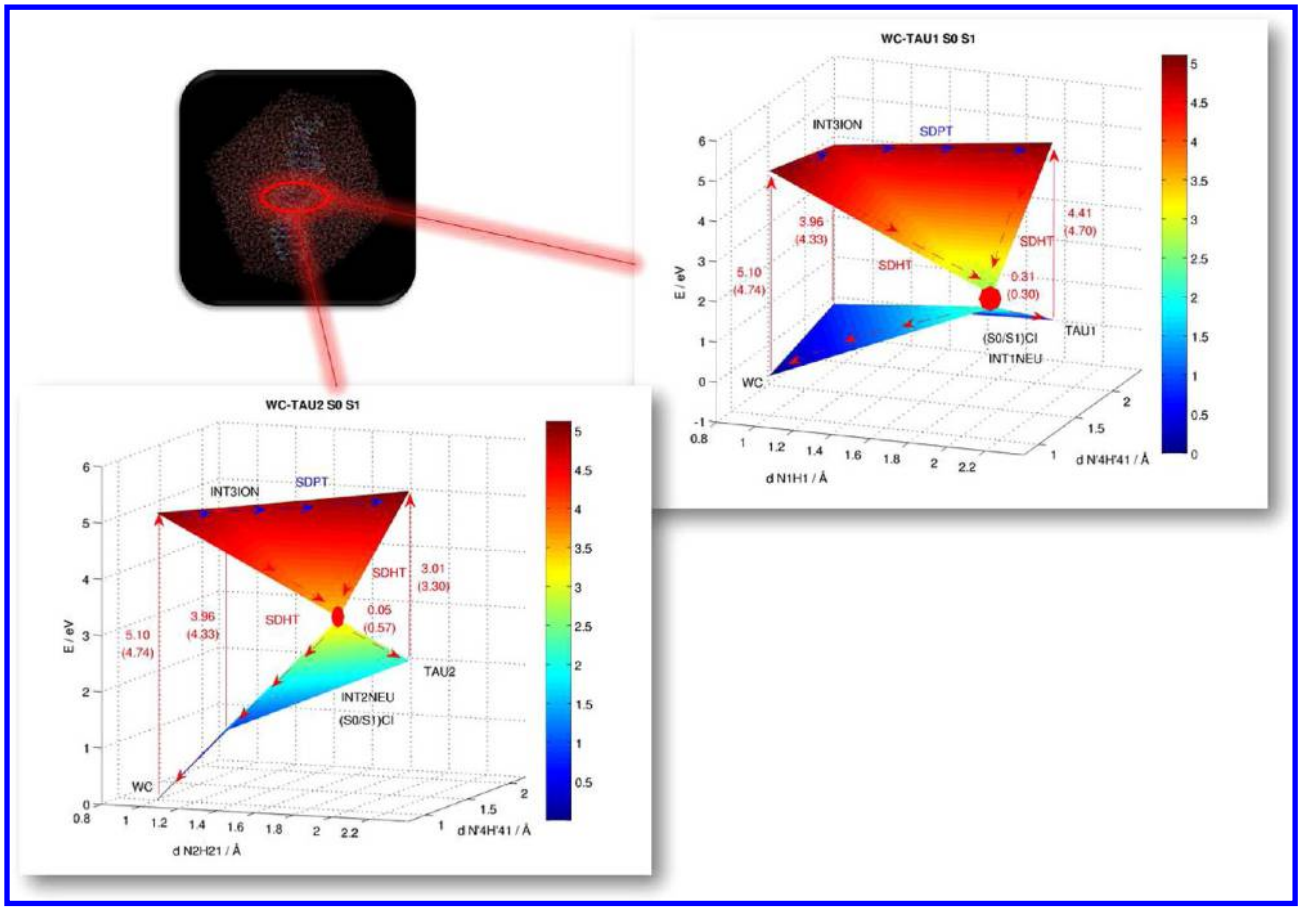

Figure 10. Stepwise double proton-transfer (SDPT) and stepwise double hydrogen-transfer (SDHT) mechanisms in the DNA-embedded GC base pair $[d(GC)_9 \cdot d(GC)_9]$ between the canonical WC form and the tautomeric TAU1 (top) and TAU2 (bottom) species. CASPT2 vertical energies (in eV) for the lowest-lying excited state (S_1) are shown, together with the related gas-phase values (within parentheses). S_1 corresponds to a locally excited state (LE) in the WC, INT3ION, and TAU1 structures and to the charge transfer state (CT) in the INT1NEU and INT2NEU systems. In TAU2, the nature of S_1 differs from the results *in vacuo*.

phase and in a DNA-embedded GC base pair. We focus on the main structures of the two stepwise mechanisms obtained *in vacuo*. Hence, the equilibrium structures of the WC, INT1NEU, INT2NEU, INT3ION, TAU1, and TAU2 species in a $d(GC)_9 \cdot d(GC)_9$ strand in aqueous solution have been determined at the CASSCF/MM level of theory. Regarding the INT1ION structure, as explained in the previous section, the optimized LE state has a higher energy than the CT state (cf. Figure 3), and consequently the SDHT mechanism via the INT1NEU intermediate (Figure 6) is activated after the $(S_1/S_2)_X$ region. Therefore, the intermediates INT1NEU, INT2NEU, and INT3ION, together with the canonical and tautomeric arrangements of the base pair, are sufficient to analyze the effects of the biological environment on the main decay channels.

Figure 10 illustrates the general scenario for the SDPT and SDHT channels in the DNA, compiling the CASPT2 energies for the ground (S_0) and lowest-lying excited (S_1) states, together with the corresponding values in the gas phase. The lowest-lying excited state at the DNA-embedded WC GC base pair corresponds to a local excitation (LE), as in the isolated base pair. DNA vertical energies are in general close to the gas phase results, which points to similar properties of the SDPT and SDHT mechanisms in both the gas and DNA phases. Crucial structures in the SDHT mechanism are the intermediates INT1NEU or INT2NEU, which are located in the region of near-degeneracy between the S_0 and S_1 PESs. The energy gap of 0.3 eV, found *in vacuo* for the INT1NEU intermediate, is preserved in the DNA, whereas the INT2NEU equilibrium structure is even closer to the CI in the biological environment. The INT3ION species, which has an ionic structure, is slightly stabilized in DNA. However, such stabilization is not sufficient to facilitate an internal conversion process *via* the SDPT mechanism. In summary, the GC base pair in both the gas phase and in DNA manifests similar attributes for the proton/hydrogen-transfer processes. A similar invariance of the photoreactivity to changes in the environment, vacuo vs DNA, has been observed for cyclobutane cytosine dimers.[117]

In light of the present QM/MM results, we expect the excited state proton/hydrogen-transfer processes of the GC base pair to be a plausible photochemical channel for the photostability of DNA and the production of tautomers. The SDHT decay will compete with the monomeric nonradiative photochemical channel, also with intrastrand phenomena such as the formation of exciplexes between π-stacked NABs, as suggested by experiments in alternating and nonalternating GC oligonucleotides[89,91] and previous computations on related systems.[52,63,118] The efficiency of the hydrogen/proton energy-decay pathways in DNA will depend on the degree of hydrogen-bonding between the strands.

Excited-State Dynamics of the GC Base Pair. Post in vacuo and DNA computations including dynamical and statistical aspects are next considered. This is in order to evaluate

dx.doi.org/10.1021/ct3006166 | J. Chem. Theory Comput. 2013, 9, 481−496

Table 1. NH Bond Lengths and Scalar Projections of the Velocities of the H_{41}', H_1, and H_{21} Atoms over the Lines Defined by the $N_4'H_{41}'\cdots O_6$, $N'_3\cdots H_1N_1$, and $O'_2\cdots H_{21}N_2$ Hydrogen Bonds, Respectively[a]

[a]	bond length/Å			projected velocity/au				
simulation	$N_4'H_{41}'$	N_1H_1	N_2H_{21}	H_{41}'	H_1	H_{21}	mechanism activated	photochemistry
Sim1	1.26	0.92	0.99	0.0032	0.0005	−0.0006		nonradiative decay *via* CI of G
Sim2	1.20	1.02	0.99	0.0028	0.0030	−0.0004	SDHT	photostability GC/TAU1 formation
Sim3	0.97	0.87	1.14	0.0008	0.0006	0.0041	SDHT	photostability GC/TAU1 formation
Sim4	1.05	1.07	1.20	0.0017	0.0042	−0.0035	SDHT	photostability GC/TAU1 formation

[a]Simulations Sim1, Sim2, Sim3, and Sim4 correspond to the structures 37, 27, 38, and 191 generated as initial conditions (see SI). [a]The mechanisms and photochemical decay paths observed in the simulations are indicated.

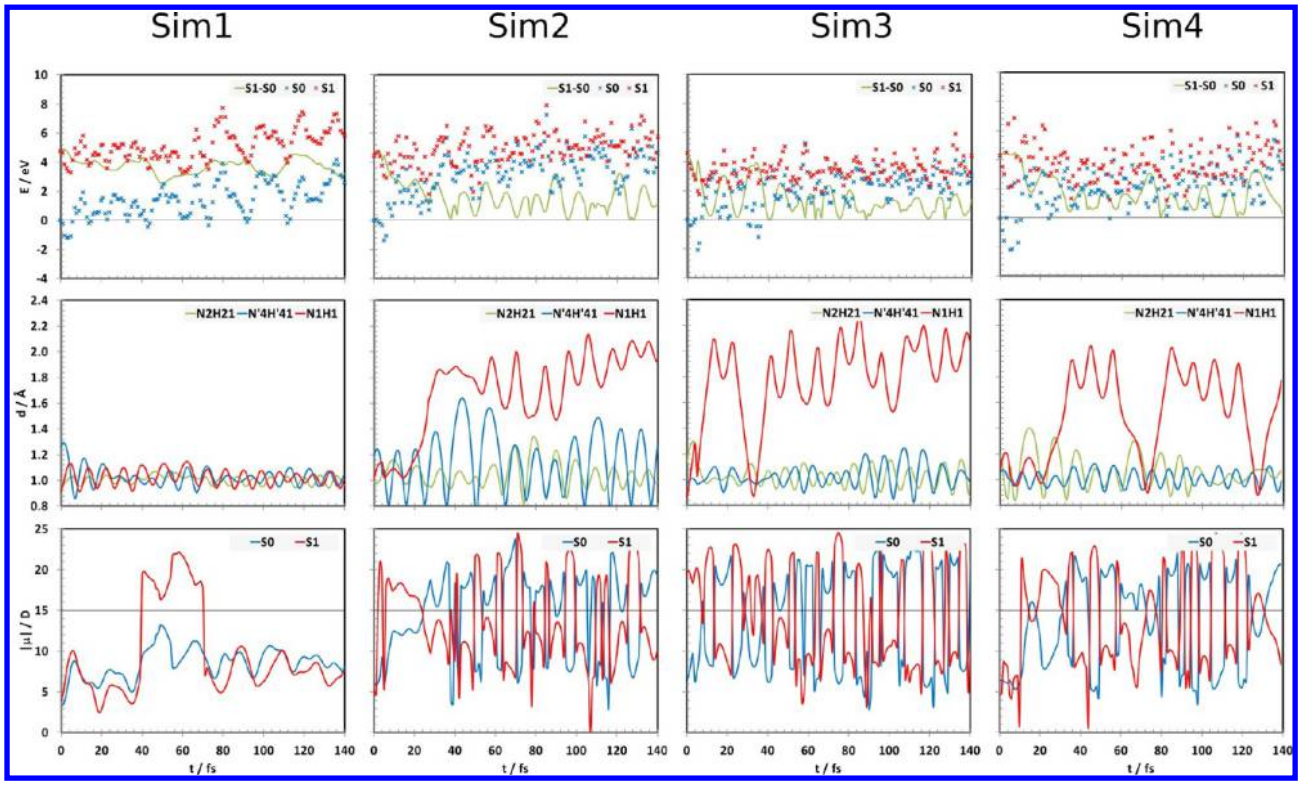

Figure 11. CASPT2 energies (E) for the ground state (S_0), the lowest-lying excited state (S_1), and energy difference between both states (S_1-S_0); NH distances (d); and the magnitude of the dipole moments ($|\mu|$) of states S_0 and S_1 vs time (t) plotted for the semiclassical dynamics simulations *Sim1*, *Sim2*, *Sim3*, and *Sim4*. CASSCF energies are displayed in Figures S8−S11.

some qualitative attributes related to the different energy-decay channels. Previous works on the dynamics of the system have not been able to achieve the correct electronic structure of the states in the FC region, and the population of the lowest-lying excited state with CT character is enhanced as an artifact of the low level of theory used.[85,93] Therefore, those earlier computations provide a qualitative incomplete description of the overall photochemistry. Here, we have performed four dynamic simulations employing the methodology used in the in vacuo and DNA computations to get a qualitative insight into the dynamical properties of the proton/hydrogen-transfer phenomenon in the GC base pair, leaving for the future a full study able to compute quantitative quantum yields for the formation of the products.

Table 1 compiles the values of the $N_4'H_{41}'$, N_1H_1, and N_2H_{21} bond lengths and projected scalar velocities of the H_{41}', H_1, and H_{21} atoms over the lines defined by the three hydrogen bonds for four initial conditions which have been selected, among a Wigner distribution of 300 points, to perform the dynamics simulations. These selected conditions have appropriate NH distances and H momenta for the analysis of some dynamical attributes of the different relaxation mechanisms of the GC base pair (radiationless decay through the G moiety, hydrogen/proton transfer *via* the SDPT or SDHT mechanisms and formation of tautomers). Figure 11 displays the results obtained for the magnitude of the dipole moments ($|\mu|$) of the ground (S_0) and low-lying excited (S_1) states; the $N_4'H_{41}'$, N_1H_1, and N_2H_{21} bond lengths; and the S_0, S_1, and S_1-S_0 energies. These properties allow us to identify the relaxation mechanism which takes place in each one of the simulations. In particular, $|\mu|$ can be used to analyze the electronic structure of the system along the simulations. In the FC region, large values ($|\mu| > 15$ D) indicate a CT nature of the states, whereas low values ($|\mu| = 0-15$ D) correspond to LE excitations. This behavior is inverted at the intermediates region in which a proton is exchanged between the NABs. Meanwhile, the NH bond distances and the energy difference between the S_0 and S_1 states gives information on the region of the PESs where the system is located.

The dynamics *simulation 1* (*Sim1*) features small momenta along the $N'_3\cdots H_1N_1$ and $O'_2\cdots H_{21}N_2$ hydrogen bonds and a large value at the $N_4'H_{41}'\cdots O_6$ site, which favors initially the

dx.doi.org/10.1021/ct3006166 | J. Chem. Theory Comput. 2013, 9, 481−496

formation of the excited state tautomeric forms *via* the SDPT mechanism (see Figures 4 and 5). However, along the simulation, the system does not show any proton/hydrogen exchange between both NABs in the base pair. The CT nature of S_1 is reached at around 40 fs (large dipole moment in Figure 11) due to a slight increase in the N_1H_1 bond distance. Subsequently, the system comes back to the region of LE character where it is relaxed toward the equilibrium structure of this LE state. From this point, the ultrafast decay path through the CI localized in the G monomer can be expected.[37] This decay pathway has not been found in the trajectories performed by Groenhof et al.,[85] due to the fact that all the simulations were started in the *CT* state, as a result of the lower level of theory employed. *Simulation 2* (*Sim2*) includes additionally an initial velocity component in the direction of the $N'_3\cdots H_1N_1$ hydrogen bond, favoring also the radiationless energy decay toward the TAU1 species or the restored WC base pair, *via* the SDHT mechanism (Figure 6). In this case, the GC base pair has a different fate. The system, initially on the S_1-LE state, evolves in a few femtoseconds into the S_1-CT state. At 25 fs, an inversion of the dipole moments of the ground and excited states takes place. Simultaneously, the H atom is transferred from G to C. Hence, the INT1NEU structure is reached, although the relaxation toward the ground state surface would not be still possible since the energy difference between the states is large. The $(S_0/S_1)_{CI}$ crossing is reached around 40 fs. It is worth noting that after this point the system is trapped in the INT1NEU structure and there is a high probability for internal conversion. Groenhof et al. obtained a recovery of the WC configuration in 75% of 20 simulations.[85] In five out of 20 runs, the TAU1 configuration was found. *Simulation 3* (*Sim3*) points to the ground-state formation of TAU2, instead of TAU1, *via* the SDHT mechanism (Figure 7). The calculation starts already with CT character of the excited state (see dipole moments of S_1 in Figure 11). Furthermore, although that a large momentum is located initially in the $O'_2\cdots H_{21}N_2$ direction pointing toward C, the hydrogen that is transferred from G to C is again H_1. The GC base pair reaches the INT1NEU configuration in a few femtoseconds, in agreement with the steep energy gradient which characterizes the S_1-CT state in the surroundings of this intermediate (see Figure 6). After the first 40 fs and a third hydrogen transfer at the center hydrogen bond, the system is trapped in the well of the INT1NEU. Large changes in the CASSCF and CASPT2 energies for the S_0 and S_1 states take place initially, and later the S_1-S_0 energy difference becomes small. The fourth calculation performed on the dynamics of the UV-irradiated GC base pair, *simulation S4* (*Sim4*), is characterized by significant initial momenta of the H atoms in all three hydrogen bonds. Over 10 fs, both ground and excited states have a low dipole moment, meaning a trapping of the system in the LE region. Later, the evolution toward CT nature takes place, a large increase of the N_2H_{21} bond length appears, and the energy difference between the S_0 and S_1 states drops dramatically. The SDHT mechanism *via* the INT2NEU intermediate seems to be activated. In fact, the ground and excited state dipole moments show an inversion. However, once the N_2H_{21} distance reaches a maximum value of 1.4 Å, the dimer distributes the kinetic energy among the other vibrational modes, and finally the SDHT mechanism *via* the INT1NEU structure is turned on instead. At 35 fs, all the control properties, i.e., magnitudes of the dipole moments, N_1H_1 distance, and vertical relative energy between S_0 and S_1, point simultaneously to the formation of the INT1NEU intermediate. Despite the simulation showing an oscillatory pattern in the hydrogen transfer, there is a window at 30−60 fs, where the system might exhibit a nonadiabatic process toward the ground-state PES.

In general, the hydrogen transfer at the $N_3'\cdots H_1N_1$ hydrogen bond is the most favorable mechanism in the four simulations carried out. The formation of the INT2NEU intermediate, which involves a hydrogen transfer at the $O_2'\cdots H_{21}N_2$ position, has not been obtained. INT1NEU requires less than 50 fs to be generated, which is a much faster process than the energy deactivation along the flat PES of the G base up to the methanamine-like CI, previously estimated around 100 fs.[37] This difference in the lifetime of both processes is probably a consequence of the fact that the former phenomenon involves the motion of mainly one H atom and that the PES is steep, while the energy relaxation toward the CI of the monomer implies out-of-plane distortions of the six-member ring along a flat PES. Tunneling effects, not considered in the employed semiclassical approach, can be expected to decrease the lifetimes. Regarding comparisons with experiments, the present results must be used with caution. Although lifetimes shorter than the energy decays in the G and C mononucleotides were measured by means of fluorescence upconversion techniques,[86] de La Harpe et al.[89] obtained energy decays an order of magnitude larger with respect to the building blocks. This suggests the formation of relatively stable excited state species by means of π-stacking interactions, which are not modeled here. The long-lived exciplexes, as a consequence of π-stacking, are however sensitive to deuterium substitution at the hydrogen bonds, showing therefore that proton/hydrogen transfers are still present.[90,91] Qualitative predictions for these processes can be established from our calculations. At the time of UV irradiation of the GC base pair, those molecules with a certain momentum in the $N'_3\cdots H_1N_1$ direction (for instance, *Sim2* and *Sim4*) might undergo a double hydrogen-transfer process, resulting in the production of the TAU1 configuration or restoring the WC structure. On the other hand, other samples with low momenta in the hydrogen atoms from the hydrogen bonds (for instance, *Sim1*) will relax the energy through the CI funnel localized in the G molecule, as pointed out in previous studies on the isolated molecule,[37] or form relatively stable exciplexes *via* the π-stacking network.[86]

SUMMARY AND CONCLUDING REMARKS

DNA photoreactivity includes processes originated in the single NABs and phenomena involving intrastrand and interstrand dimers.[92] Photoinduced proton/hydrogen-transfer processes in the GC base pair have been studied in the present contribution with the well-established quantum-chemistry CASSCF/CASPT2 method, complementing previous works on the ultrafast non-radiative energy decay in NABs[38] and the UV-induced formation of photodimers in π-stacked dimers.[52,63] Three different mechanisms have been introduced as possible candidates for energy decay in the base pair: (1) stepwise double proton transfer, SDPT, (2) stepwise double hydrogen transfer, SDHT, and (3) concerted double proton transfer, CDPT. On the basis of the present findings, SDHT is potentially the most favorable mechanism to explain the photostable properties of the canonical GC base pair and also the formation of tautomers (see Figure 12). In the SDHT mechanism, proton motions at the $N'_3\cdots H_1N_1$ or $O'_2\cdots H_{21}N_2$ sites favor the evolution of the lowest-lying excited state from LE to CT character. Subsequently, this CT nature of the state drives a hydrogen transfer to form the INT1NEU and INT2NEU intermediates, respectively. These species are located in a region of near degeneracy with the ground-state surface,

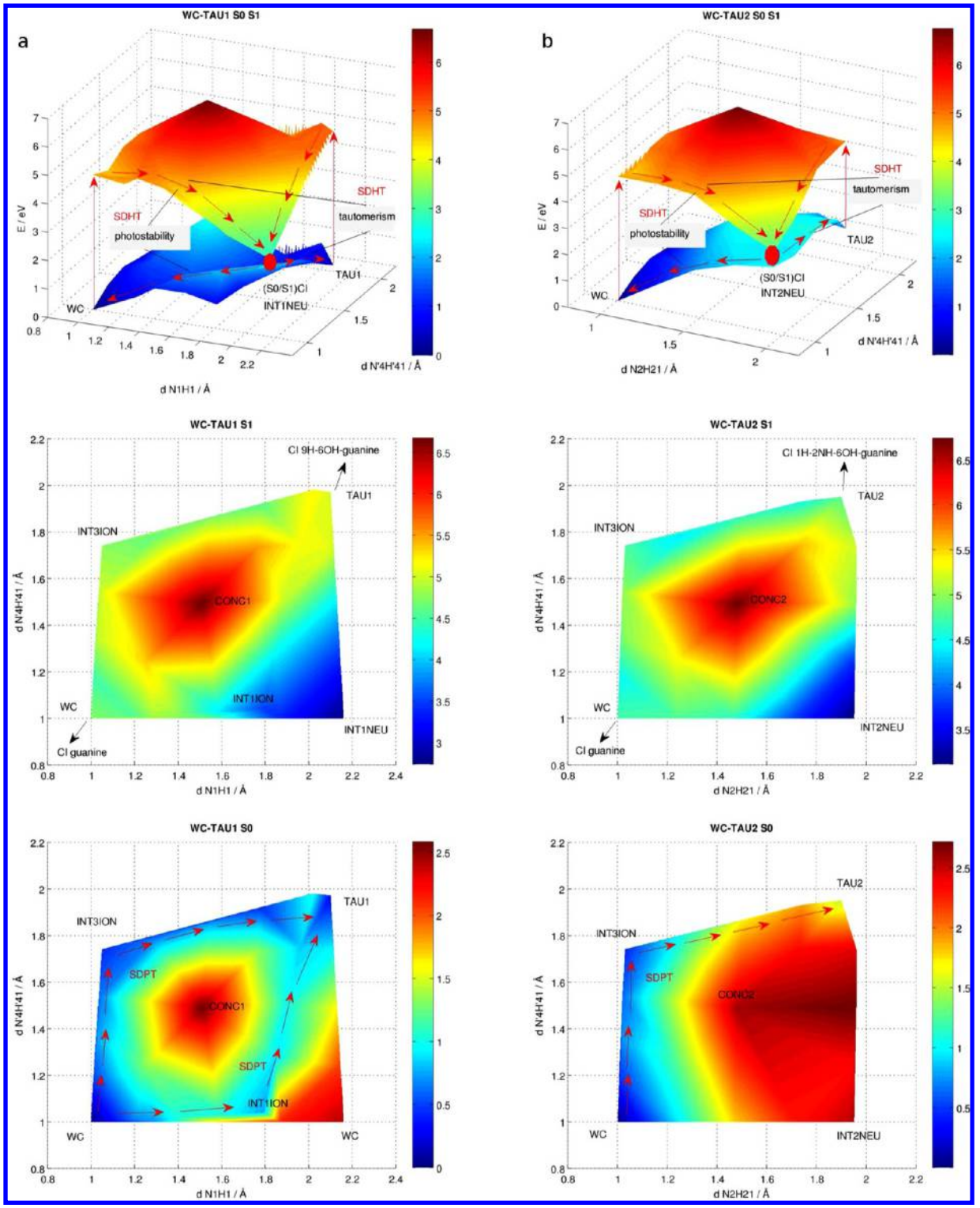

Figure 12. GC base pair PESs of the ground (S_0) and lowest-lying excited state (S_1) for the GC base pair along the stretching NH reaction coordinates to form the TAU1 (a) and TAU2 (b) tautomeric forms. The relative position of the intermediate structures (INT1NEU, INT2NEU, INT1ION, INT3ION, CONC1, and CONC2) between the Watson−Crick (WC) configuration and the tautomers is shown. The most favorable paths connecting the WC and TAU1/TAU2 species in the S_0 and S_0−S_1 PESs are displayed in red (SDPT and SDHT, respectively). Additional energy-decay paths in the WC, TAU1, and TAU2 species are indicated by black arrows. Energies (in eV) are relative to the ground-state equilibrium structure of the WC GC base pair.

which can funnel the reaction path toward the restored WC GC base pair or a tautomeric new form *via* a second hydrogen transfer at the same or a different interbase-pair hydrogen bond, respectively. Tautomers TAU1 and TAU2 can be produced in such a manner during the UV irradiation of the GC base pair. Analogous SDHT processes apply to the tautomeric forms, resulting in the canonical base pair or restoring the tautomers (cf. Figure 12). TAU2 is a high-energy configuration among the GC base pairs studied, with the lowest energy barrier to restore the WC form. According to the energy profiles obtained, thermal

dx.doi.org/10.1021/ct3006166 | *J. Chem. Theory Comput.* 2013, 9, 481−496

conversions are more favorable *via* the SDPT mechanism, as compared to SDHT and CDPT.

In solution with polar solvents, the SDHT mechanism is presumably altered, inactivating the internal conversion channel, which brings the WC GC base pair back to its ground state equilibrium structure or to new tautomeric configurations.[96] However, the DNA-embedded GC dimer studied by the QM/MM computational approach manifests the same qualitative behavior for the double proton/hydrogen-transfer processes as *in vacuo*. This supports experimental observations[86,90,91] and previous theoretical predictions[85,93] pointing to the proton/hydrogen transfer as a relevant process in the photochemistry of DNA duplexes. Considering the post-UV-irradiation dynamics of the system, the GC base pair evolves toward either the LE minimum or to the INT2NEU intermediate produced *via* the SDHT mechanism. As for the former, it might decay to the ground-state WC structure *via* the CI of the G nucleobase ($CI_{guanine}$ in Figure 12). Regarding the hydrogen-transfer phenomenon, it seems to be more prone along the center hydrogen bond. Lifetimes for the hydrogen transfer (around 50 fs) are found to be much shorter than the nonradiative decays localized on the monomers. Nevertheless, a direct comparison with the experimental measurements is not possible, since intrastrand photochemical processes, such as the formation of exciplexes, might affect this property (lifetimes), as suggested by Kohler and co-workers.[89,91]

In general, new photochemical routes are accessible in the UV-irradiated GC base pair, which will compete with the energy-decay pathways of the isolated NABs and π-stacked (or intrastrand) dimers. The former process will be more efficient in highly hydrogen-bonding conformations of the DNA double helix. Vibrations at the hydrogen bonds can activate hydrogen/proton transfers in the GC base pair, as suggested by the simulated dynamics of the system. The operative mechanism for decay is expected to be a double hydrogen transfer, which provides the system with new photostable channels, in addition to those present in the isolated NABs. However, the formation of tautomers (DNA photoreactivity) is also possible *via* the double hydrogen transfer. These noncanonical GC base pairs have analogous relaxation mechanisms, which have not been previously considered. The new findings might be important for the interpretation of the experimental data and the design of new experiments aimed to further understand the role of hydrogen transfer in the excited-state dynamics of the DNA. The C-based imino-enol tautomer is both photochemically and thermally unstable, which is a beneficial property for the preservation of the genetic code, since this species may originate replication breakdowns and consequently interrupt the proper cell function. Meanwhile, the formation of the highly stable C-based imino-oxo tautomer may induce GC→AT transitions in the replication process with relevant repercussions in evolutionary biology.

■ ASSOCIATED CONTENT

Supporting Information

CASSCF active-space orbitals, CASPT2 energies and Mulliken charges, CASSCF interbase-pair hydrogen bond distances *in vacuo*, computational details of the classical dynamics simulations, details of plotting of Figures 2−7, Wigner distribution, and CASSCF energies for the semiclassical dynamics simulations. This information is available free of charge via the Internet at http://pubs.acs.org/.

■ AUTHOR INFORMATION

Corresponding Author

*E-mail: Vicenta.Sauri@uv.es, jpgobbo@iq.usp.br, Daniel.Roca@kvac.uu.se.

Notes

The authors declare no competing financial interest.

■ ACKNOWLEDGMENTS

This work was supported by projects CTQ2007-61260, CTQ2010-14892, and CSD2007-0010 Consolider-Ingenio in Molecular Nanoscience of the Spanish MICINN/FEDER. J.P.G. thanks CAPES (Coordenação de Amparo ao Pessoal de Ensino Superior, Project 2272/09-1) and FAPESP (Fundação de Amparo à Pesquisa do Estado de São Paulo, Project 2010/16043-2) for postdoctoral fellowships. M.L. thanks the Marcus and Amalia Wallenberg foundation for financial support. P.B.C. thanks financial support from projects CTQ2009-07120 (MICINN) and UAH2011/EXP-041 (UAH). A.C.B. thanks FAPESP and CNPq (Conselho Nacional de Desenvolvimento Científico e Tecnológico) for financial support. R.L. thanks the Swedish Research Council (VR) for financial support. J.J.S.-P. and D.R.-S. are grateful for support from the European Research Council under the European Community's Seventh Framework Programme (FP7/2007-2013)/ERC grant agreements no. 251955 and 255363, respectively. The services and computer time made available by the Servei de Informàtica de la Universitat de València, the Laboratório de Computação Científica Avançada (LCCA) of the Universidade de São Paulo, and the UPPMAX center of the University of Uppsala are also acknowledged.

■ REFERENCES

(1) Dahm, R. *Hum. Genet.* **2008**, *122*, 565−581.
(2) Watson, J. D.; Crick, F. H. C. *Nature* **1953**, *171*, 737−738.
(3) Bixon, M.; Giese, B.; Wessely, S.; Langenbacher, T.; Michel-Beyerle, M. E.; Jortner, J. *Proc. Natl. Acad. Sci. U.S.A.* **1999**, *96*, 11713−11716.
(4) Adleman, L. M. *Science* **1994**, *266*, 1021−1024.
(5) Mikhailopulo, I. A.; Miroshnikov, A. I. *Mendeleev Commun.* **2011**, *21*, 57−68.
(6) *Radiation Induced Molecular Phenomena in Nucleic Acids. A Comprehensive Theoretical and Experimental Analysis*; Leszczynski, J., Shukla, M., Eds.; Springer: The Netherlands, 2008.
(7) *DNA Repair and Mutagenesis*; Friedberg, E. C., Walker, G. C., Siede, W., Wood, R. D., Schultz, R. A., Ellenberger, T., Eds.; ASM Press: Washington DC, 2006.
(8) Colson, A. O.; Sevilla, M. D. In *Computational Molecular Biology*; Leszczynski, J., Ed.; Elsevier: Amsterdam, 1999; Vol. *8*, pp 245−270.
(9) Cadet, J.; Vigny, P. In *Bioorganic Photochemistry*; Morrison, H., Ed.; John Wiley & Sons: New York, 1990; Vol. *1*, pp 1−272.
(10) Björn, L. O.; McKenzie, R. L. In *Photobiology. The Science of Life and Light*; Björn, L. O., Ed.; Springer: New York, 2008; pp 503−530.
(11) Douki, T; Cadet, J. *Biochemistry* **2001**, *40*, 2495−2501.
(12) *Computational Molecular Biology*; Leszczynski, J., Ed.; Elsevier: Amsterdam, 1999.
(13) *Theoretical Biochemistry. Processes and Properties in Biological Systems*; Eriksson, L. A., Ed.; Elsevier: Amsterdam, 2001.
(14) Fu, L.-Y.; Wang, G.-Z.; Ma, B.-G.; Zhang, H.-Y. *Biochem. Biophys. Res. Commun.* **2011**, *409*, 367−371.
(15) Fromme, J. C.; Banerjee, A.; Verdine, G. L. *Curr. Opin. Struct. Biol.* **2004**, *14*, 43−49.
(16) Braithwaite, E. K.; Prasad, R.; Shock, D. D.; Hou, E. W.; Beard, W. A.; Wilson, S. H. *J. Biol. Chem.* **2005**, *280*, 18469−18475.
(17) Ismail, N.; Blancafort, M.; Olivucci, M.; Kohler, B.; Robb, M. A. *J. Am. Chem. Soc.* **2002**, *124*, 6818−6819.

(18) Merchán, M.; Serrano-Andrés, L. *J. Am. Chem. Soc.* **2003**, *125*, 8108−8109.
(19) Matsika, S. *J. Phys. Chem. A* **2004**, *108*, 7584−7590.
(20) Marian, C. M. *J. Chem. Phys.* **2005**, *122*, 104314.
(21) Tomic, K.; Tatchen, J.; Marian, C. M. *J. Phys. Chem. A* **2005**, *109*, 8410−8418.
(22) Perun, S.; Sobolewski, A. L.; Domcke, W. *J. Am. Chem. Soc.* **2005**, *127*, 6257−6265.
(23) Blancafort, L.; Cohen, B.; Hare, P. M.; Kohler, B.; Robb, M. A. *J. Phys. Chem. A* **2005**, *109*, 4431−4436.
(24) Chen, H.; Li, S. H. *J. Phys. Chem. A* **2005**, *109*, 8443−8446.
(25) Nielsen, S. B.; Sølling, T. I. *ChemPhysChem* **2005**, *6*, 1276−1281.
(26) Zgierski, M. Z.; Patchkovskii, S.; Lim, E. C. *J. Chem. Phys.* **2005**, *123*, 081101.
(27) Zgierski, M. Z.; Patchkovskii, S.; Fujiwara, T.; Lim, E. C. *J. Phys. Chem. A* **2005**, *109*, 9384−9387.
(28) Merchán, M.; González-Luque, R.; Climent, T.; Serrano-Andrés, L.; Rodríguez, E.; Reguero, M.; Peláez, D. *J. Phys. Chem. B* **2006**, *110*, 26471−26476.
(29) Serrano-Andrés, L.; Merchán, M.; Borin, A. C. *Proc. Natl. Acad. Sci. U.S.A.* **2006**, *103*, 8691−8696.
(30) Perun, S.; Sobolewski, A. L.; Domcke, W. *J. Phys. Chem. A* **2006**, *110*, 13238−13244.
(31) Blancafort, L. *J. Am. Chem. Soc.* **2006**, *128*, 210−219.
(32) Chen, H.; Li, S. H. *J. Chem. Phys.* **2006**, *124*, 154315.
(33) Gustavsson, T.; Banyasz, A.; Lazzarotto, E.; Markovitsi, D.; Scalamani, G.; Frisch, M. J.; Barone, V.; Improta, R. *J. Am. Chem. Soc.* **2006**, *128*, 607−619.
(34) Serrano-Andrés, L.; Merchán, M.; Borin, A. C. *Chem.—Eur. J.* **2006**, *12*, 6559−6571.
(35) Marian, C. M. *J. Phys. Chem. A* **2007**, *111*, 1545−1553.
(36) Zgierski, M. Z.; Patchkovskii, S.; Lim, E. C. *Can. J. Chem.* **2007**, *85*, 124−134.
(37) Serrano-Andrés, L.; Merchán, M.; Borin, A. C. *J. Am. Chem. Soc.* **2008**, *130*, 2473−2484.
(38) Yamazaki, S.; Domcke, W.; Sobolewski, A. L. *J. Phys. Chem. A* **2008**, *112*, 11965−11968.
(39) Lan, Z.; Fabiano, E.; Thiel, W. *ChemPhysChem* **2009**, *10*, 1225−1229.
(40) Serrano-Andrés, L.; Merchán, M. *J. Photochem. Photobiol. C: Photochem. Rev.* **2009**, *10*, 21−32.
(41) González-Vázquez, J.; González, L. *ChemPhysChem* **2010**, *11*, 3617−3624.
(42) Barbatti, M.; Szymczak, J. J.; Aquino, A. J. A.; Nachtigallová, D. *J. Chem. Phys.* **2011**, *134*, 014304.
(43) Crespo-Hernandez, C. E.; Cohen, B.; Hare, P. M.; Kohler, B. *Chem. Rev.* **2004**, *104*, 1977−2019.
(44) Samoylova, E.; Lippert, H.; Ullrich, S.; Hertel, I. V.; Radloff, W.; Schultz, T. *J. Am. Chem. Soc.* **2005**, *127*, 1782−1786.
(45) Canuel, C.; Mons, M.; Piuzzi, F.; Tardivel, B.; Dimicoli, I.; Elhanine, M. *J. Chem. Phys.* **2005**, *122*, 074316.
(46) Kuimova, M. K.; Dyer, J.; George, M. W.; Grills, D. C.; Kelly, J. M.; Matousek, P.; Parker, A. W.; Sun, X. Z.; Towrie, M.; Whelan, A. M. *Chem. Commun.* **2005**, 1182−1184.
(47) Daniels, M.; Hauswirt, W. *Science* **1971**, *171*, 675−677.
(48) Hauswirt., W; Daniels, M. *Photochem. Photobiol.* **1971**, *13*, 157−163.
(49) Hauswirt., W; Daniels, M. *Chem. Phys. Lett.* **1971**, *10*, 140−142.
(50) Callis, P. R. *Chem. Phys. Lett.* **1979**, *61*, 563−567.
(51) Callis, P. R. *Annu. Rev. Phys. Chem.* **1983**, *34*, 329−357.
(52) Crespo-Hernández, C. E.; Cohen, B.; Kohler, B. *Nature* **2005**, *436*, 1141−1144.
(53) Markovitsi, D.; Onidas, D.; Gustavsson, T.; Talbot, F.; Lazzarotto, E. J. *J. Am. Chem. Soc.* **2005**, *127*, 17130−17131.
(54) Kwok, W. M.; Ma, C. S.; Phillips, D. L. *J. Am. Chem. Soc.* **2006**, *128*, 11894−11905.
(55) Buchvarov, I.; Wang, Q.; Taytchev, M.; Trifonov, A.; Fiebig, T. *Proc. Natl. Acad. Sci. U. S. A.* **2007**, *104*, 4794−4797.
(56) Takaya, T.; Su, C.; De La Harpe, K.; Crespo-Hernández, C. E.; Kohler, B. *Proc. Natl. Acad. Sci. U. S. A.* **2008**, *105*, 10285−10290.
(57) Miannay, F. A.; Banyasz, A.; Gustavsson, T.; Markovitsi, D. *J. Am. Chem. Soc.* **2007**, *129*, 14574−14575.
(58) Santoro, F.; Barone, V.; Improta, R. *Proc. Natl. Acad. Sci. U. S. A.* **2007**, *104*, 9931−9936.
(59) Schreier, W. J.; Schrader, T. E.; Koller, F. O.; Gilch, P.; Crespo-Hernández, C. E.; Swaminathan, W. N.; Carell, T.; Zinth, W.; Kohler, B. *Science* **2007**, *315*, 625−629.
(60) Boggio-Pasqua, M.; Groenhof, G.; Schafer, L. V.; Grubmuller, H.; Robb, M. A. *J. Am. Chem. Soc.* **2007**, *129*, 10996.
(61) Blancafort, L.; Migani, A. *J. Am. Chem. Soc.* **2007**, *129*, 14540−14541.
(62) Roca-Sanjuán, D.; Olaso-González, G.; González-Ramírez, I.; Serrano-Andrés, L.; Merchán, M. *J. Am. Chem. Soc.* **2008**, *130*, 10768−10779.
(63) Olaso-González, G.; Merchán, M.; Serrano-Andrés, L. *J. Am. Chem. Soc.* **2009**, *131*, 4368−4377.
(64) González-Ramírez, I.; Roca-Sanjuán, D.; Climent, T.; Serrano-Pérez, J. J.; Merchán, M.; Serrano-Andrés, L. *Theor. Chem. Acc.* **2011**, *128*, 705−711.
(65) Douki, T; Cadet, J. *Biochemistry* **2001**, *40*, 2495−2501.
(66) Abo-Riziq, A.; Grace, L.; Nir, E.; Kabelac, M.; Hobza, P.; de Vries, M. S. *Proc. Natl. Acad. Sci. U.S.A.* **2005**, *102*, 20−23.
(67) Lowdin, P. O. *Rev. Mod. Phys.* **1963**, *35*, 724−732.
(68) Lowdin, P. O. *Adv. Quantum Chem.* **1965**, *2*, 213−360.
(69) Douhal, A.; Kim, S. K.; Zewail, A. H. *Nature* **1995**, *378*, 260−263.
(70) Chachisvilis, M.; Fiebig, T.; Douhal, A.; Zewail, A. H. *J. Phys. Chem. A* **1998**, *102*, 669−673.
(71) López-Martens, R.; Long, P.; Sogaldi, D.; Soep, B.; Syage, J.; Millie, P. *Chem. Phys. Lett.* **1997**, *273*, 219−226.
(72) Takeuchi, S.; Tahara, T. *Chem. Phys. Lett.* **1997**, *227*, 340−346.
(73) Folmer, D. E.; Poth, L.; Wisniewski, E. S.; Castleman, A. W., Jr. *Chem. Phys. Lett.* **1998**, *287*, 1−7.
(74) Kwon, O. H.; Zewail, A. H. *Proc. Natl. Acad. Sci. U. S. A.* **2007**, *104*, 8703−8708.
(75) Schwalb, N. K.; Temps, F. *J. Am. Chem. Soc.* **2007**, *129*, 9272−9273.
(76) Douhal, A.; Guallar, V.; Moreno, M.; Lluch, J. M. *Chem. Phys. Lett.* **1996**, *256*, 370−376.
(77) Moreno, M.; Douhal, A.; Lluch, J. M.; Castaño, O.; Frutos, L. M. *J. Phys. Chem. A* **2001**, *105*, 3887−3893.
(78) Catalán, J.; del Valle, J. C.; Kasha, M. *Chem. Phys. Lett.* **2000**, *318*, 629−636.
(79) Serrano-Andrés, L.; Merchán, M. *Chem. Phys. Lett.* **2006**, *418*, 569−575.
(80) Sobolewski, A. L.; Domcke, W.; Hattig, C. *Proc. Natl. Acad. Sci. U. S. A.* **2005**, *102*, 17903−17906.
(81) Frutos, L. M.; Markmann, A.; Sobolewski, A. L.; Domcke, W. *J. Phys. Chem. B* **2007**, *111*, 6110−6112.
(82) Sobolewski, A. L.; Domcke, W. *Phys. Chem. Chem. Phys.* **2004**, *6*, 2763−2771.
(83) Yamazaki, S.; Taketsugu, T. *Phys. Chem. Chem. Phys.* **2012**, *14*, 8866−8877.
(84) Shukla, M. K.; Leszczynski, J. *J. Phys. Chem. A* **2002**, *106*, 4709−4717.
(85) Groenhof, G.; Schäfer, L. V.; Boggio-Pasqua, M.; Goette, M.; Grubmüller, H.; Robb, M. A. *J. Am. Chem. Soc.* **2007**, *129*, 6812−6819.
(86) Markwick, P. R.; Doltsinis, N. L.; Schlitter, J. *J. Chem. Phys.* **2007**, *126*, 045104.
(87) Markwick, P. R.; Doltsinis, N. L. *J. Chem. Phys.* **2007**, *126*, 175102.
(88) Miannay, F.-A.; Bányász, Á.; Gustavsson, T.; Markovitsi, D. *J. Am. Chem. Soc.* **2007**, *129*, 14574−14575.
(89) Crespo-Hernández, C. E.; de La Harpe, K.; Kohler, B. *J. Am. Chem. Soc.* **2008**, *130*, 10844−10845.
(90) Doorley, G. W.; McGovern, D. A.; George, M. W.; Towrie, M.; Parker, A. W.; Kelly, J. M.; Quinn, S. J. *Angew. Chem., Int. Ed.* **2009**, *48*, 123−127.

(91) de La Harpe, K.; Crespo-Hernández, C. E.; Kohler, B. *J. Am. Chem. Soc.* **2009**, *131*, 17557−17559.
(92) Middleton, C. T.; de La Harpe, K.; Su, C.; Law, Y. K.; Crespo-Hernández, C. E.; Kohler, B. *Annu. Rev. Phys. Chem.* **2009**, *60*, 217−239.
(93) Alexandrova, A. N.; Tully, J. C.; Granucci, G. *J. Phys. Chem. B* **2010**, *114*, 12116−12128.
(94) Vayá, I.; Miannay, F. A.; Gustavsson, T.; Markovitsi, D. *ChemPhysChem* **2010**, *11*, 987−989.
(95) Vayá, I.; Changenet-Barret, P.; Gustavsson, T.; Zikich, D.; Kotlyar, A. B.; Markovitsi, D. *Photochem. Photobiol. Sci.* **2010**, *9*, 1193−1195.
(96) Biemann, L.; Kovalenko, S. A.; Kleinermanns, K.; Mahrwald, R.; Markert, M.; Improta, R. *J. Am. Chem. Soc.* **2011**, *133*, 19664−19667.
(97) Andersson, K.; Malmqvist, P.-Å.; Roos, B. O. *J. Chem. Phys.* **1992**, *96*, 1218−1226.
(98) Roos, B. O.; Andersson, K.; Fülscher, M. P.; Malmqvist, P.-Å.; Serrano-Andrés, L.; Pierloot, K.; Merchán, M. *Adv. Chem. Phys.* **1996**, *93*, 219−331.
(99) Merchán, M.; Serrano-Andrés, L. In *Computational Photochemistry*; Olivucci, M., Ed.; Elsevier: Amsterdam, 2005.
(100) Serrano-Andrés, L.; Merchán, M. In *Encyclopedia of Computational Chemistry*, Schleyer, P. v. R., Schreiner, P. R., Schaefer, H. F., III, Jorgensen, W. L., Thiel, W., Glen, R. C., Eds.; Wiley: Chichester, U. K., 2004.
(101) Roca-Sanjuán, D.; Aquilante, F.; Lindh, R. *WIREs: Comput. Mol. Sci.* **2012**, *2*, 585−603.
(102) Aquilante, F.; De Vico, L.; Ferre, N.; Ghigo, G.; Malmqvist, P. A.; Neograd y, P.; Pedersen, T. B.; Pitonak, M.; Reiher, M.; Roos, B. O.; Serrano-Andrés, L.; Urban, M.; Veryazov, V.; Lindh, R. *J. Comput. Chem.* **2010**, *31*, 224−247.
(103) Pierloot, K.; Dumez, B.; Widmark, P.-O.; Roos, B. O. *Theor. Chim. Acta* **1995**, *90*, 87−114.
(104) Moughal Shahi, A. R.; Cramer, C. J.; Gagliardi, L. *Phys. Chem. Chem. Phys.* **2009**, *11*, 10964−10972.
(105) Gobbo, J. P.; Sauri, V.; Roca-Sanjuán, D.; Serrano-Andrés, L.; Merchán, M.; Borin, A. C. *J. Phys. Chem. B* **2012**, *116*, 4089−4097.
(106) Forsberg, N.; Malmqvist, P.-Å. *Chem. Phys. Lett.* **1997**, *274*, 196−204.
(107) Cornell, W. D.; Cieplak, P.; Bayly, C. I.; Gould, I. R.; Merz, K. M.; Ferguson, D. M.; Spellmeyer, D. C.; Fox, T.; Caldwell, J. W.; Kollman, P. A. *J. Am. Chem. Soc.* **1995**, *117*, 5179−5197.
(108) Cheatham, T. E., III; Cieplak, P.; Kollman, P. A. *J. Biomol. Struct. Dyn.* **1999**, *16*, 845.
(109) Andersen, H. C. *J. Comput. Phys.* **1983**, *52*, 24−34.
(110) Stålring, J.; Bernhardsson, A.; Lindh, R. *Mol. Phys.* **2001**, *99*, 103−114.
(111) Barbatti, M.; Granucci, G.; Persico, M.; Ruckenbauer, M.; Vazdar, M.; Eckert-Maksic, M.; Lischka, H. *J. Photochem. Photobiol. A: Chem.* **2007**, *190*, 228−240.
(112) Wigner, E. *Phys. Rev.* **1932**, *40*, 0749−0759.
(113) Frisch, M. J.; Trucks, G. W.; Schlegel, H. B.; Scuseria, G. E.; Robb, M. A.; Cheeseman, J. R.; Scalmani, G.; Barone, V.; Mennucci, B.; Petersson, G. A.; Nakatsuji, H.; Caricato, M.; Li, X.; Hratchian, H. P.; Izmaylov, A. F.; Bloino, J.; Zheng, G.; Sonnenberg, J. L.; Hada, M.; Ehara, M.; Toyota, K.; Fukuda, R.; Hasegawa, J.; Ishida, M.; Nakajima, T.; Honda, Y.; Kitao, O.; Nakai, H.; Vreven, T.; Montgomery, J. A., Jr.; Peralta, J. E.; Ogliaro, F.; Bearpark, M.; Heyd, J. J.; Brothers, E.; Kudin, K. N.; Staroverov, V. N.; Kobayashi, R.; Normand, J.; Raghavachari, K.; Rendell, A.; Burant, J. C.; Iyengar, S. S.; Tomasi, J.; Cossi, M.; Rega, N.; Millam, J. M.; Klene, M.; Knox, J. E.; Cross, J. B.; Bakken, V.; Adamo, C.; Jaramillo, J.; Gomperts, R.; Stratmann, R. E.; Yazyev, O.; Austin, A. J.; Cammi, R.; Pomelli, C.; Ochterski, J. W.; Martin, R. L.; Morokuma, K.; Zakrzewski, V. G.; Voth, G. A.; Salvador, P.; Dannenberg, J. J.; Dapprich, S.; Daniels, A. D.; Farkas, Ö.; Foresman, J. B.; Ortiz, J. V.; Cioslowski, J.; Fox, D. J. *Gaussian 09*, revision A.1; Gaussian, Inc.: Wallingford, CT, 2009.
(114) Perun, S.; Sobolewski, A. L.; Domcke, W. *J. Chem. Phys. A* **2006**, *110*, 9031.
(115) Dargiewicz, M.; Biczysko, M.; Improta, R.; Barone, V. *Phys. Chem. Chem. Phys.* **2012**, *14*, 8981−8989.
(116) Roca-Sanjuán, D.; Rubio, M.; Merchán, M.; Serrano-Andrés, L. *J. Chem. Phys.* **2006**, *125*, 084302.
(117) Roca-Sanjuán, D.; Olaso-González, G.; Rubio, M.; Coto, P. B.; Merchán, M.; Ferré, N.; Ludwig, V.; Serrano-Andrés, L. *Pure App. Chem.* **2009**, *81*, 743−754.
(118) Olaso-González, G.; Merchán, M.; Serrano-Andrés, L. *J. Am. Chem. Soc.* **2009**, *131*, 4368−4377.